ELSEVIER

Biophysical Chemistry 125 (2007) 32–49

Biophysical Chemistry

http://www.elsevier.com/locate/biophyschem

Photophysics of ANS. IV. electron transfer quenching of ANS in alcoholic solvents and mixtures

William Kirk *, William Wessels

Mayo Foundation, Rochester, MN 55902, United States

Received 18 January 2006; received in revised form 26 July 2006; accepted 31 July 2006
Available online 12 August 2006

Abstract

ANS is observed to decay from the fluorescent state with distributed kinetics in nearly pure ethanol solvent, notwithstanding that in mixed ethanol/water solvents the decay is discrete and biexponential. The origin of this behavior is investigated. In particular, a theory of electron transfer theory in the adiabatic regime is adduced, with specific involvement of solvent cage structure in the form of the solvent–electron *polaron* wave function. Properties of various polarons for various solvent systems are predicted and, for the case of ethanol and cyclohexanol, employed to generate the observed Arrhenius-type decay parameters in a quantitative fashion.
Published by Elsevier B.V.

Keywords: 1, 8 ANS; Morse polaron; Distributed fluorescence decay; Electron transfer to solvent

1. Introduction

It is sometimes of interest to revisit older investigations with newer apparatus, if only just to see how older results stand up to newer approaches and technique. We confront the fluorescence lifetime decay characteristics of ANS in ethanol/water mixtures, in cyclohexanol, dioxane, and dioxane/water mixture, and peripherally in glycerol/water mixtures in this report (for ethanol/water solutions cf. [1]; for dioxane cf. [2]). These experimental conditions were chosen because there already exists a large literature on precisely these systems, and also because of similarities to the gross spectroscopic features of some typical ANS–protein complexes.

Specifically, we observe in ethanol/water mixtures the following perplexing behavior: At low water activity (<10 mol%), there is a clear *distribution* of lifetimes, with a fairly substantial width. This gives way at 10 mol% water to a decay characterized by two distinct single exponential decay terms – attempted fitting to distributions yielding very small widths for either component – both decay times being substantially longer than the corresponding lifetime in pure water. Lastly, in pure water, one regains the very short single lifetime previously observed by ourselves and many others.

Now, distributed lifetimes are hardly unique to ANS decay kinetics, but the *pattern* observed here is rather surprising. If we can obtain some insight into the origin and properties of this distributed lifetime, it might be helpful in analyzing situations with protein-complexed ANS, or other fluorophores, such as *trp* residues in proteins, which seem often to have distributions that change shape, e.g., becoming narrower or broader, for reasons which have so far proven elusive.

To be precise: a (Gaussian) distributed decay is such that, for excited molecule '*A*', the decay distribution is given by:

$$A(t,k) = A_0(0)/\left[(2\pi)^{1/2}\sigma\right]\exp(-(k-k_0)^2/2\sigma_k^2)\exp(-kt) \quad (1a)$$

with the total decay function with time being an integration of the amplitude $A(t,k)$

$$\langle A(t)\rangle = \int \mathrm{d}k A(t,k) \quad (1b)$$

and hence:

$$\ln(A(t)) = \ln(A_0(0)) - k_0 t + \sigma_k^2 t^2/2 + \ln(1+\mathrm{erf}(\sigma_k t - k_0)) \quad (1c)$$

There are several ways this kind of distribution could arise. Either 1) the decay process in question arises from a Gaussian-distributed set of initial states, each of which has an effective

* Corresponding author.
E-mail address: kirk.william@mayo.edu (W. Kirk).

0301-4622/$ - see front matter. Published by Elsevier B.V.
doi:10.1016/j.bpc.2006.07.019

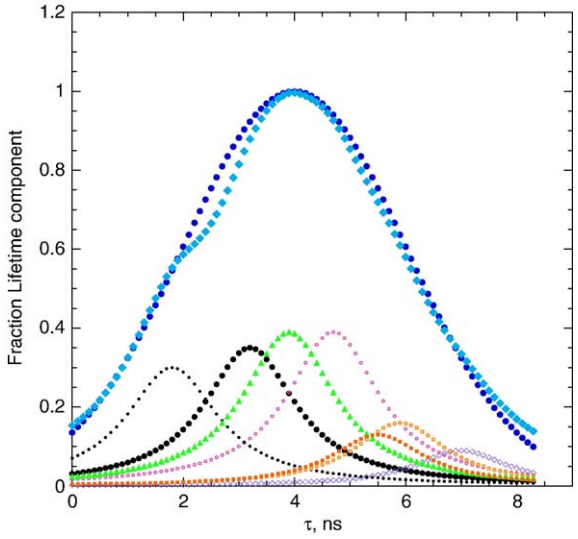

Fig. 1. Hypothetical 'Gaussian'-distributed decay decomposed as an inhomogeneous distributed sum of Lorentzian subdecays. The *homogeneously* distributed decay is treated in this contribution.

transition rate given by a quantum-mechanical (squared matrix element) term, or sum of terms – this might be called the inhomogeneously distributed decay; or 2) there is one single quantum state, but it is subject to a chemical – not quantal – rate process exhibiting (a) static disorder, a statically, Gaussian distributed set of barriers which do not interconvert on the timescale of the lifetime, or (b) dynamically disordered kinetics, e.g. diffusion of the system, leading to distributed k's – this can be called dynamically distributed decay (cf. Zwanzig [3]). There is yet another kind of distributed decay of a homogeneous initial state, most apparent in isolated molecules, as discussed by Lin and Eyring [4] which is due to energy dispersion of the initial or final states, or in the presence of 'coherence' between initial and final state vibrational modes. These effects are expected to be small or even unobservable in condensed phases, because of largely complete collisional decoherence. For the rest of this paper, we will neglect this latter effect.

To illustrate, Fig. 1 shows a 'Gaussian' decay distribution which *might* be composed of a sum of different decays – each with their own widths, however, which would themselves still have to be explained. But, we could also have a single decaying state whose decay is *homogeneously* broadened, as are each of the component Lorentzians in the figure, but now in the overall shape of a Gaussian.

So, when do we talk of a single decaying state, as opposed to a number of, or even a distribution of such states? Phenomenologically, when there is a coupled rate equation with two or more eigenvalues, these represent two or more decaying states. But to what does this situation correspond *physically*? In ordinary spectroscopy, one can have a single excited state of a charged oscillator with a strong interaction, say, with the *e–m* field, and a well defined, maximum probable energy, yet, because of being "dressed" by weak interactions with the environment, the precise energy of an emerging photon is uncertain, being broadened by the damping of the oscillator these weak interactions bring about. Similarly in dynamics, it ought to be the case that a single excited state characterized by a strong interaction with the environment (leading to decay), produced by a function of time, say, $G_1(t_0 \rightarrow t_1;\ A \rightarrow B)$ [5] nonetheless might have a fairly imprecisely determined *decay time*. Consider perhaps that 'pure' B state is not the ultimate (irreversible) decay product, but that weak secondary interactions bring about a "dressing" of B: G_2 $(t_2 \rightarrow \infty,\ t_2 > t_1;\ B \rightarrow b)$ where the various 'b' substrates are the products, but each of them can arise only from B. So these weak secondary interactions, or correlations, are the means by which the total decay probability factors into two conditional probabilities. Thus the key to obtaining a homogeneously distributed decay is the existence of a separation of time scales of the most significant dynamics of an ensemble of decaying systems (perhaps a quantum wave packet) from the dynamics of more detailed effects which characterize any particular decaying system [6]. At some point the wave packet of a quantum system is resolved into a particular semi-classical system, and the system has irreversibly decayed. As we will describe the process in this study, an electron becomes a *polaron* on its way to *solvated* status.

The dominant temperature dependent, and hence, nuclear momentum dependent, decay mechanism for ANS we will assume to be electron transfer to solvent. This should come as no surprise, since a large number of authors have considered it [1,2,7–10]. More surprising to us, however, is our finding herein that the main coupling of this solvent–solute energy fluctuation to the electron transfer (e.t.) event, which is called the reorganization energy in the Marcus–Levich–Dogonadze theory of e.t. [11], does not control the distribution of decay constants. Continuous fluctuation of charge distributions in a solute and in the solvent produce a kind of 'Brownian motion' of the solvent–solute interaction, giving rise to a smooth Gaussian distribution of solvation energies (or particle–bath coupling energies) [12] and, in the case of electron transfer, *this very process is intimately linked with the excited state decay process*

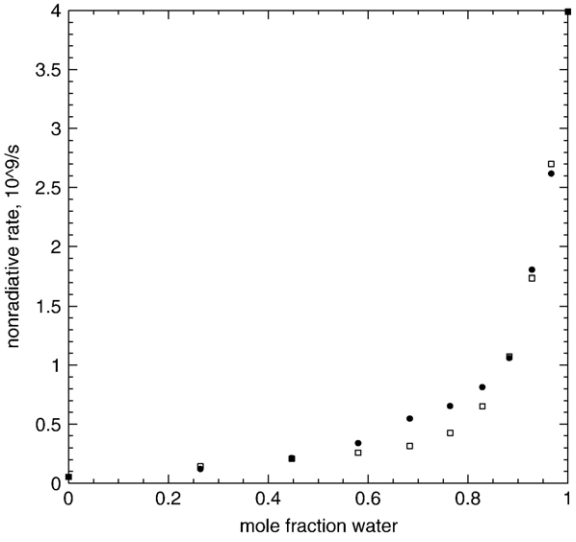

Fig. 2. Decay rate constant of ANS in ethanol/H_2O mixtures as a function of added water; data from Robinson et al. [1]. Filled squares: here replotted by mole fraction of water. Open squares are fitting to a 13° binomial described in text.

itself. One readily imagines that this process will distribute the rate constant for a single quantal state, in the above sense. In fact that conjecture would be false, as will be seen in the body of this paper, for we show that the linkage of this process to the dynamics of electron transfer does not, in itself, produce any distribution of rate constant for the electron transfer. It is the diffusion of the solvent cage of the successor electron (called a polaron), a cage induced in the solvent by the electron itself, which takes place on a different time scale from the electron's motion, which is the origin of our broadening, we surmise.

Robinson et al. [1] worked with EtOH/water mixtures and found a very steep dependence of nonradiative decay rate with volume fraction of water. We have replotted their data as mole fraction of water in EtOH in Fig. 2. Now, we have attempted to fit this data with a number of models proportional to the mole fraction of water. If it were significant, say, that a single site near ANS be occupied with H_2O, generating a *fast* rate, and otherwise occupied generating a *slow* rate, then as a mole fraction of water or χ we would have:

$$\text{Rate} = \chi k_{\text{fast}} + (1-\chi)k_{\text{slow}} \tag{2a}$$

If two waters were necessary at one site we could have:

$$\text{Rate} = \chi^2 k_{\text{fast}} + (1-\chi^2)k_{\text{slow}}; \tag{2b}$$

or, if there were two sites we might expect some intermediate form:

$$\text{Rate} = \chi^2 k_{\text{fast}} + (1-\chi)^2 k_{\text{slow}} + 2\chi(1-\chi)k_{\text{intermed}}, \quad \text{and so on.} \tag{2c}$$

In this way we tried to generate the *form* which could duplicate the results given. We do not obtain anything like the steep dependence observed with any less than 13 water molecules. That is, we have taken a form $\chi^{13}k_{\text{fast}}+13\chi^{12}(1-\chi)k_{\text{inter},12}+78\chi^{11}(1-\chi)^2 k_{\text{inter},11}+286\chi^{10}(1-\chi)^3 k_{\text{inter},10}+715\chi^9(1-\chi)^4 k_{\text{inter},9}+1287\chi^8(1-\chi)^5 k_{\text{inter},8}+1716\chi^7(1-\chi)^6 k_{\text{inter},7}+\cdots(1-\chi)^{13}k_{\text{slow}}$; where all the k_{inter} values are of the order of k_{slow} (in the plot, we used $k_{\text{inter},n}=(1+n/2)k_{\text{slow}}$).

This is more than just an idle exercise, we insist. It severely constrains what type of physical model one can employ in predicting decay rates. There has to be one rate characteristic of pure water, when present in a rather sizable cluster about the ANS, and very much smaller rates characteristic of inhomogeneous solvent clusters (or disordered clusters), with one or more ethanol molecules inserted. And the eventual mechanism must yield a smoothly distributed rate in nearly pure ethanol solutions, in the experimental results we produce below.

We develop, then, our model to generate a smoothly distributed decay rate in nearly pure ethanol, which *naturally* evolves into a disordered system as the mole-fraction of water is increased. This disordering then naturally produces a localization of the decay-products, which leads to a *discrete* set of decays. We invoke an ANS structure characteristic of the highly aqueous phase *distinct* from the structure in a nonaqueous phase (i.e., we invoke a difference in rotameric states found in NMR solution structures [13], see also Part V in this series) to explain the occurrence of two distinct lifetimes in these mixtures. Lastly, we attempt to explain the magnitude of the decay constants in pure water and pure ethanol – their Arrhenius prefactors and energies. Along the way we make predictions about the nature of the decay constants in cyclohexanol and dioxane, which are at least partially borne out.

2. Materials and methods

Fluorescence lifetime measurements were performed using a time-correlated single-photon counting fluorometer. The frequency-doubled output of a Coherent Antares 76S YAG mode-locked laser drove a Coherent 700 dye laser with an attached Coherent 7220 cavity dumper. Rhodamine 6G dye was employed in the Coherent 700, and the laser was tuned to 600 nm for pulsed excitation. The pulse-width was approximately 2 ps with a 3.8 MHz rep. rate. The output of the dye laser was frequency-doubled to 300 nm with a BBO crystal second-harmonic generator. Emission from the sample compartment was passed through a 10-nm interference filter centered at 360 nm and a Glan–Thompson polarizing prism set at the magic angle. A Hamamatsu R2809 multichannel plate photomultiplier tube was used for detection. Two ZFL-1000LN Mini-Circuits amplifiers in series with a −10 dB attenuator processed the NCP signal for use with a Tennelec 454 constant fraction discriminator (CFD), which produced a 'Start' signal for a Tennelec 864 time–amplitude converter (TAC) and biased amplifier. The 'Stop' signal to the TAC was produced by sampling the dye laser output with a Lasermetrics 3117PD PIN diode. Its output was then amplified via a ZFL-1000LN and processed by a Tennelec 454 CFD.

Absolute ethanol was obtained from Aaper (Shelbyville, KY), and used directly. Dioxane was from Burdick and Jackson (Madison, WI) or Fluka (Ronkonkoma, NY) and used directly. No difference was observed in data at 15 °C and 25 °C obtained from the two solvent sources. As a further check, the dioxane from Burdick and Jackson was passed over a neutral silical gel drying column (Woelm. Eschwege F.R.G.), was centrifuged to remove suspended silica gel particles, and used. Again, no differences at 15 °C and 25 °C were obtained. For the rest of the temperature dependence, the Fluka dioxane was employed. Cyclohexanol was also obtained from Fluka. We employed two solutions of ethanol in water of very low water activity, 1 mol% and 3 mol% (<0.3% by volume and <1% by volume) in order to be able to extrapolate to *zero* water activity, since it is notoriously difficult to work with and maintain water-free and spectroscopically 'clean' conditions with ethanol. Moreover the results from Robinson et al. [1] were compelling to them that they had obtained *single exponential* decays in pure ethanol. Although they may not have attempted to fit to Gaussian decay distributions, our results are equally compelling to us that single, *discrete*, exponential behavior is not the case.

We prepared 2 different mixtures of glycerol/water at 70 vol. % glycerol and 80 vol.% glycerol. As we were interested in obtaining species-associated-spectra in these mixtures, we utilized a set of interference filters from 470 nm to 580 nm

with roughly 10 nm band-pass each to collect emission with high wavelength discrimination.

3. Experimental results

We carried out studies of the temperature dependence of the fluorescence decay of ANS in various ethanolic solutions. Fig. 3a and b show our results fitted to a simple Gaussian distribution model of the decay–time profiles for 1 mol% and 3 mol% water in ethanol. The effective decay rate 'k' was calculated as $\langle\tau\rangle^{-1}$, where $\langle\tau\rangle$ is given by:

$$\langle\tau\rangle = \tau_0 + \sigma_t/\sqrt{\pi}\, e^{-\tau_0^2/2\sigma^2} \tag{3}$$

These results were subjected to further analysis. We took each 'k' to be the sum of a temperature-dependent and temperature

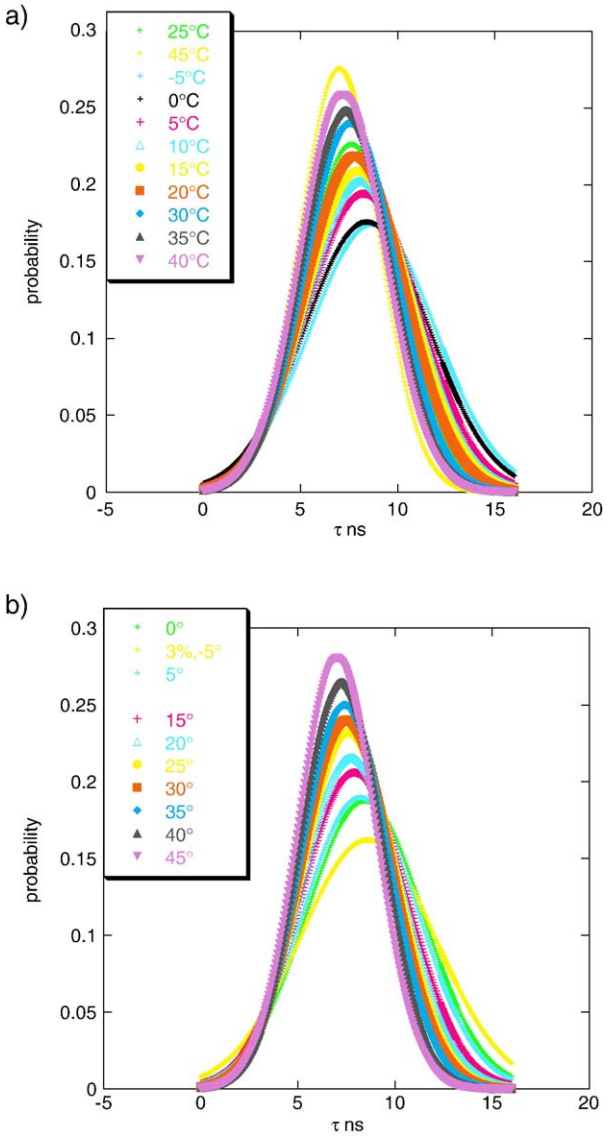

Fig. 3. Fluorescence decay distributions as obtained by us in 1% H_2O in ethanol (a), and 3% H_2O in ethanol (b); these are plotted for the temperature range of −5 °C to 40 °C, with 5 °C increments.

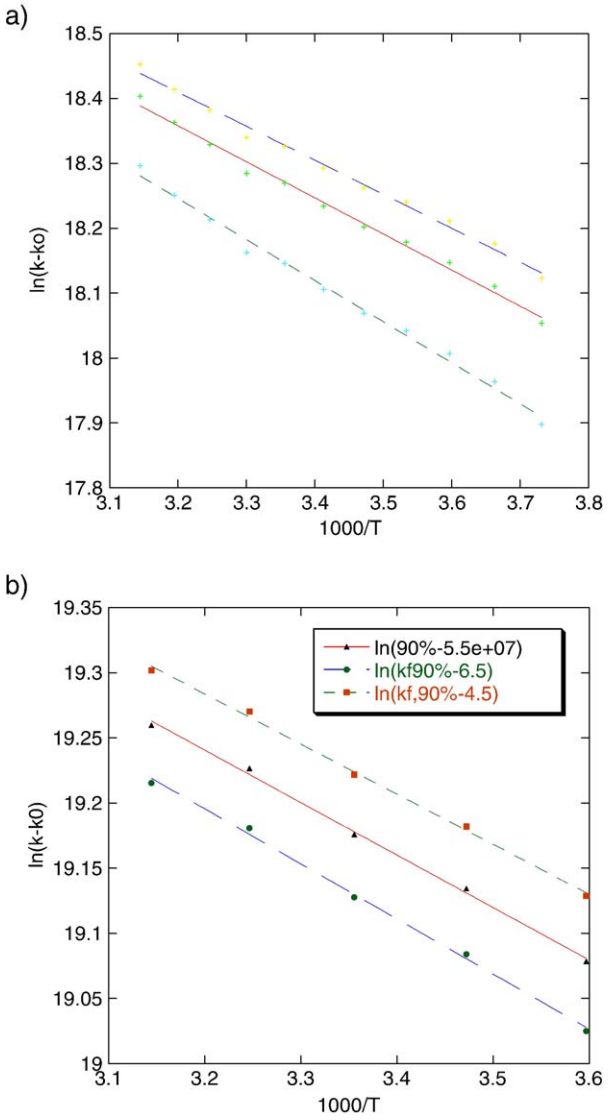

Fig. 4. (a) Arrhenius plot for 1% water in ethanol data, for following choices of k_0, see text: 4.0×10^7 s^{-1}, 4.5×10^7 s^{-1} and 5.5×10^7 s^{-1}; slopes are −0.52, −0.56, and −0.63, respectively, and the natural logarithm of the Arrhenius prefactors are 20.09, 20.14, and 20.27, respectively, with correlation coefficient=.996 and $\chi^2\sim0.0009$ for each fit. (b) Arrhenius plot for 10% water in ethanol. Choices of k_0 are 4.5×10^7 s^{-1}, 5.5×10^7 s^{-1}, and 6.5×10^7 s^{-1}, respectively, natural logarithm of Arrhenius prefactors are 20.51, 20.53, and 20.55, respectively (slopes are 0.40±0.02) with correlation coefficient=0.9987 and $\chi^2\sim5\times10^{-5}$ for each fit. Beyond the range of k_0 indicated, the χ_2 values and/or correlation coefficients are substantially worse.

independent part. Thus we fit the following expression for a range of values of k_{indep}:

$$\ln(k-k_{\text{indep}}) = \ln A - \Delta E_A^{\ddagger}/RT \tag{4}$$

In Fig. 4, we show the best fit for a number of choices of k_{indep} for the 1% data. There is an unambiguous range of best values of k_{indep}, beyond which, either if chosen too high or too low, both the parameters of goodness of fit, namely χ^2 and the correlation coefficient becomes worse. For 1% and 3%, this range is roughly $k_{\text{indep}}=4.5\pm0.5\times10^7\text{s}^{-1}$. One can compare this with the

Table 1
Decay times of ethanol/water mixtures

T (K)	480 nm emission (50 mol% EtOH)				520 nm emission (50 mol% EtOH)				540 nm emission (50 mol% EtOH)				490 nm emission 90 mol% EtOH				
	τ_1	x_1	τ_2	$\langle\tau\rangle$	τ_1	x_1	τ_2	$\langle\tau\rangle$	τ_1	x_1	τ_2	$\langle\tau\rangle$		τ_1	x_1	τ_2	$\langle\tau\rangle$
278	2.09	.748	.405	1.67	2.10	.853	.607	1.88	2.08	.883	.619	1.91	278	4.38	.916	.583	4.06
288	1.95	.818	.564	1.70	1.94	.879	.783	1.80	1.92	.911	.566	1.80	288	4.11	.927	.645	3.85
293	1.84	.846	.454	1.63	1.82	.935	.719	1.75	1.81	.956	.044	1.76	298	3.91	.942	.868	3.73
303	1.78	.831	.710	1.61	1.78	.869	.958	1.67	1.71	.897	.251	1.59	308	3.75	.945	1.035	3.60
313	1.68	.861	.815	1.56	1.63	.925	.640	1.56	1.59	.938	.300	1.51	318	3.60	.947	1.02	3.46

All decay times are in nanoseconds. χ^2 values for all fits were less than 1.25.

expected rates of radiative decay. Robinson et al. [1] found the QY of ANS in pure ethanol to be 0.41. Others [2] found a value of 0.40. The radiative rate can then be calculated to be $\sim 5\times10^7$ s^{-1}. This is quite close to the value calculated via the Strickler–Berg formula, and essentially the same as k_{indep}. Thus, if there is any contribution to the temperature independent rate from intersystem crossing, it must be quite small.

The values found for the Arrhenius prefactor for 1%, and 3% water in ethanol are $5.3\pm1.1\times10^8$ s^{-1} and $5.0\pm0.5\times10^8$ s^{-1}, respectively. The slopes of the Arrhenius plots were found to be $-0.52\pm0.06\times1000R$ and $-0.55\pm.06\times1000R$, respectively.

We also concluded studies with 90 mol% ethanol plus water, and 50 mol% ethanol/water. Fig. 4b shows the Arrhenius fitting for $k_{\text{indep}}=4.5\times10^7$ s^{-1} for the 90% data. We remark that the best 'choice' for k_{indep} is $4.0\pm0.5\times10^7$ s^{-1}, which again makes for a small intersystem crossing. In the case of 90% and 50%, fits to *distributed* decay components were possible but not terribly satisfactory, yielding very narrow distributions ($\sim$0.3 ns), which are probably not distinguishable empirically from single-exponentials at the respective values at the center, or τ_0. In addition, the decays could only be fit by more than one component-exponential (the smaller contribution being the smaller lifetime, generally <1 ns). In these cases $\langle\tau\rangle$ was taken to be equal to $\sum x_i\tau_i$ (cf. Kirk et al. [14]), where the 'x_i' are the fractions of each decay component. This data is summarized in Table 1.

For the case of water, we shall simply quote the results of Robinson et al. [10] that the observed Arrhenius slope is 0, and our own results that the single lifetime of ANS in H_2O is 0.27 ns and in D_2O is 0.67 ns [15].

We also investigated the decay of ANS in cyclohexanol. This data is presented in Table 2. For cyclohexanol the lifetime data are not as clearcut as for the previous solvents. While it is true that some components seem to be robust, the longest lifetime component varies from fitting to fitting from 9 ns to 30 ns. The general pattern of the 3-component fittings does display a rough symmetry about the middle (the largest fraction) lifetime component, and thus can be recast as a rate-space Gaussian distribution fairly readily. But the fits and the χ^2 values are at times not impressive. As one can see from Table 2, the $\langle\tau\rangle^{-1}$ values seem generally to *decrease* with temperature, yet the k_0 (center of the Gaussian rate distribution) values generally *decrease* with temperature. Consequently, the Arrhenius temperature dependence, fitting to both sets of data independently, yields the rather large error in $\Delta E_A^{\ddagger}=8.5\pm8$ kJ/mol.

Decay data were obtained in dioxane and dioxane/water solutions (65 mol% dioxane) chosen to mimic the emission wavelength characteristics of ANS bound to I-FABP. In pure dioxane a single-component lifetime of 13.2 ns was found. In dioxane/water mixture with H_2O the lifetime obtained was 10.6, while in dioxane/D_2O the lifetime was 13.9. The difference between pure dioxane and dioxane/D_2O may be significant, and we have not corrected the lifetimes for differences in refractive

Table 2
Cyclohexanol decay parameters

T (K)	τ_1 (ns)	α_1	τ_2	α_2	τ_2	$\langle\tau\rangle$	χ^2	k_0 (10^8 s^{-1})	σ_k (10^8 s^{-1})
298	10.16	0.287	2.03	0.718	–	4.36	1.476	2.24	0.87
303	13.89	0.179	2.99	0.614	0.869	4.50	1.281	2.37	0.96
308	35.07	0.103	3.035	0.563	0.698	5.55	1.102	2.44	1.10
313	9.76	0.351	2.30	0.618	0.505	4.87	1.432	2.04	0.78
318	18.74	0.133	3.67	0.735	0.422	5.24	1.101	2.33	0.94
323	18.22	0.137	4.05	0.728	0.515	5.51	0.998	2.19	0.87
328	10.08	0.258	2.89	0.742	–	4.74	1.335	2.36	0.86

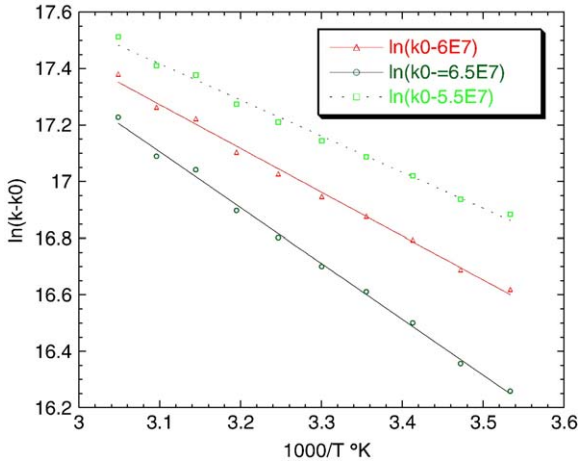

Fig. 5. Arrhenius plot for dioxane, with the following choices for k: 5.0×10^7 s^{-1}, 6.0×10^7 s^{-1} and 6.5×10^7 s^{-1}. The following slopes, natural logarithms of Arrhenius prefactors, with the resulting correlation coefficients are obtained: 1.16 and 21.15, with 0.9967; 1.63, and 22.34, with 0.9982; lastly: 2.05 and 23.47, with 0.9987, for low, medium, and high values of k_0. The χ^2 values trend in the opposite direction from the correlation coefficients.

Table 3
Solvation/redox energies of ANS

Naphthalene (ad.) I.P. 8.14 eV (1.7 V redox); 1-Aminonapthalene (0.54 V redox); *N*-phenylaniline E.A. 0.86 V; aniline E.A. (0.98 V). Hammett σ for $SO_3^- - \phi = 0.3$
Site solvation: sum in $H_2O = -90 \pm 40$ kJ/mol; in $C_6H_{11}OH = -63 \pm 30$ kJ/mol[a]
Born solvation: $(H_2O)_4^-$ (2.04 Å) = −336 kJ/mol; $(H_2O)_{12}^-$ (3.94 Å) = −174 kJ/mol; $(EtOH)_4^-$ (3.56 Å) = −187 kJ/mol; $(C_6H_{11}OH)_4^-$ (5.12 Å) = −127 kJ/mol; ANS in H_2O (6.3 Å) = −109 kJ/mol; in EtOH (7.6 Å) = −88 kJ/mol; in $C_6H_{11}OH$ (11.6 Å) = −56 kJ/mol
hν (in H_2O) = 360 nm = 334 kJ/mol; (in EtOH) = 370 nm = 325 kJ/mol; (in $C_6H_{11}OH$) = 375 nm = 321 kJ/mol
Work against solvent in assembling products: −3 kJ/mol (H_2O), −8 kJ/mol (EtOH)
Electron affinity (gas phase) $(H_2O)_4 = 25$ kJ/mol; $(H_2O)_{12} = 73$ kJ/mol
ΔF^0 Totals:
$H_2O = (8.14 - 1.16 - 0.10) \times 96.5 - 3.0 - 90 - 174 - 109 - 334 - 3 - 73 = -122 \pm 40$ kJ/mol
$EtOH = (8.14 - 1.16 - 0.10) \times 96.5 - 3.0 - 90 - 187 - 88 - 325 - 8 - 25 = -62 \pm 40$ kJ/mol
$C_6H_{11}OH = (8.14 - 1.16 - 0.10) \times 96.5 - 3.0 - 63 - 127 - 56 - 321 - 8 - 30 = -56 \pm 30$ kJ/mol

[a] Electrochemical values for naphthalenes are from Murov et al. [44]. For ethanol, we assume that site solvation is about 90 kJ/mol due to dipole–dipole interaction, polarizability and quadrupole interactions as for water, whereas we assume the dipole–dipole term is 40±30 kJ/mol for cyclohexanol and the quadrupole term is zero, with the polarizability about −23 kJ/mol as described in the text. For water, it is calculated as "soft polaron" free energy, and that of the "hard" polaron it is −236 kJ/mol.

index between the two solvents. There is actually a larger calculated k_{rad} (mostly due to the red shifting of the emission) for dioxane/water than for dioxane, but the discrepancy vis-à-vis the actual k_{rad} is also a bit larger for dioxane/water. The reasons for this behavior will be explored more closely in the next contribution. The slope of the Arrhenius plots in Fig. 5 for dioxane is equivalent to 11.5±2.5 kJ/mol. It is uncertain what the value of $\Delta F^{0\prime}$, the electrochemical free energy change of the reaction (calculated in Table 3), is for dioxane. But it is likely that the reorganization energy is not large, and that the $\Delta F^{0\prime}$ could be positive, because the Born solvation energy is not going to assume a large negative value. The value for k_{indep} is $5.5 \pm .8 \times 10^7\ s^{-1}$, which is about $1.5 \times 10^7\ s^{-1}$ more than the k_{rad}, and must, we suspect, correspond with an increased rate of intersystem crossing. The Arrhenius prefactor one obtains from these plots is about $2.5 \times 10^9\ s^{-1}$.

Lastly, we present *species-associated spectra* in Fig. 7(a–c) for two glycerol/water mixtures at two different temperatures, 40 °C and 10 °C. These experiments were conducted to address the possibility that inhomogeneities contribute to the observed decay kinetics in hydroxylic solvents. For example the delayed luminescence resulting from a caged nascently ejected electron recombining with ANS radical-cation might produce a distribution of decay times. We also conducted these experiments with red-edge excitation, at 430 nm.

For glycerol/water mixtures two decay times are generally observed, which are quite robust through the varying emission wavelengths, and characteristic for each temperature. What changes from wavelength to wavelength is the *fraction* of decay into either short or long decay channel (70%: 10 °C, 1.8±.2 ns and 0.4±.2 ns; 40 °C, 1.5±.1 ns and 0.5±.1 ns; 80%: 10 °C, 2.0±.3 ns and 1.1±.3 ns; 40 °C, 1.2±.2 ns and 0.3±.1 ns).

We now compare the observed Arrhenius parameters with those we calculate from equation and related equations (cf. Appendix B), utilizing as fitting parameter only the reorganization energy λ, all other inputs being fixed independently by theory presented below. The reorganization energy itself can be rather inaccurately approximated by

$$\lambda = (e_0^2/2)(1/R_d + 1/R_a - 1/R_{ds})[1/\varepsilon_\infty - 1/\varepsilon_0] \quad (5)$$

so that even this input can be considered as an independent, first principles-derived quantity. As is seen from Table 4, where we compare this value with the empirically best fit value, this formula overestimates the empirical value. We also obtain the expected lifetime distribution widths, according to the theory developed below.

3.1. Theory, and discussion

3.1.1. 'Distributed' electron transfer dynamics in solution: the polaron in solvent picture

The electric field (determined by the nuclear charges) and the *electron field* tend to respond on different time scales. If the electron wave oscillation is very fast compared with the nuclear motion, which then represents a quasistationary surface on which the electron wave function can be 'solved', one can envision the electron actually fluctuating back and forth between the precursor and successor states many times before the separation of the nuclear centers leads to product formation. This scenario comprises an *adiabatic* electron transfer. The other limiting case occurs when, one can imagine, the driving force is so large, and the barrier is thus so high to the primary electron transfer event, that electric field fluctuations are much faster than the electron 'wave' oscillations – this is the *nonadiabatic* case. Here one does not need to refer to the incipient products as precursor or successor – since the slow step *is* transfer, they are merely donor or acceptor products.

Table 4
Arrhenius rate parameters for solvents

	$d\ln\rho_0/d(1000/T)$	$d\ln\varepsilon_0/d(1000/T)$	E_A (diel)	ΔE_{act} (obs)	ΔF^*	ΔF^0	$\lambda_{(calc)}$	$\lambda_{(obs)}$
H_2O	0.0176	0.39	18.8	~0	2.15	−122	101	84 216
EtOH	0.126	0.412	20.5	4.3	5.2	−62	92	35
$C_6H_{12}O$	0.0789	0.879	4.2	8.5±8	2.7	−56	60	36

Energies are given in kJ/mol. Activation energy of dielectric relaxation are taken from: for water [45], for ethanol [46] for cyclohexanol [47].
The 'observed' activation energy, $\Delta E^{\ddagger}$, is from Arrhenius plots for the various solvents, as described in the text. ΔF^0 are as given in Table 3. Reorganization energies calculated according to formula (6) and as "observed" from fitting Eq. (B1b). We calculate the factor $d\ln f(T)/d(1000/T)$ as 0.0037 for ethanol, but −1.28 for cyclohexanol, 0.568 for the hard polaron in water and 0.142 for the soft polaron in water. Uncertainties for λ are ±30 kJ/mol for water and ±15 kJ/mol for ethanol and cyclohexanol. The value of 216 is for the 'hard' polaron in water, which we neglect henceforth.

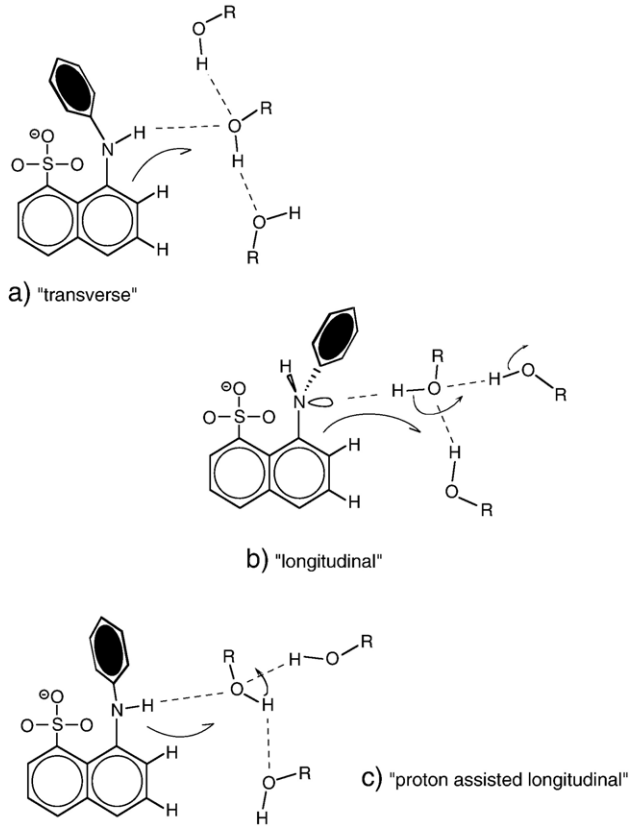

Fig. 6. Schematic illustration of (a) transverse e.t. to solvent, (b) of longitudinal e.t. (where hydrogen bonds supporting the solvent cage are broken down), and of (c) longitudinal with proton-transfer assist. A polaron can also diffuse longitudinally (by carrying waters along with it) as opposed to transversally, where the cage itself can diffuse without specific waters co-diffusing.

Song and Stuchebrukov [16] have worked out a formalism which tries to bridge the gap between the two formalisms from the nonadiabatic side. There is no formalism of which we are aware attempting to bridge from the adiabatic side – and the fully coupled model requires nonperturbational treatments. As we will see later, the case of ANS quenching in water may represent a transitional form, wherein approach to a barrier is insofar like the adiabatic formalism, but wherein no connected surface exists to the product state, which must be reached instead by a quantum transition from the closest-approach (adiabatic) surface, so that the forward rate also has nonadiabatic features.

We begin with the formula (A5b)

$$\text{Rate} = \mathrm{d}\langle N(E)\rangle/\mathrm{d}t = 4\pi\lambda/h\langle\exp(\hbar(\omega_0-\omega)//kT)\rangle\langle\exp(-(\omega_0-\omega+\lambda)^2/4k_\mathrm{B}T\lambda)\rangle \tag{6}$$

A formula similar to the 'adiabatic crossing rate' (6) can be expected to obtain even in the case of CT spectra, the thermal CT event being the limit as $\omega\to 0$. The averaging $\langle\ \rangle$ in (6) is considered to take place near the intersection of the potential energy curves for donor and acceptor states. The *centered distribution*, f^*, is defined in terms of a parameter m via the following equations:

$$\int (E_+-E_-)f^*\mathrm{d}^3\mathbf{r}^* = 0; \tag{7a}$$

$$f^* = \exp(-(E_--m(E_+-E_-))/kT)/\int \mathrm{d}^3\mathbf{r}\exp(-(E_--m(E_+-E_-))/k_\mathrm{B}T); \tag{7b}$$

Marcus [11] introduces m in several ways (as a Lagrange multiplier is probably the clearest version) – in any case m^2 is the ratio of the squared momentum, or the average kinetic energy, associated with the successor surface divided by the square of the difference momentum $(\Delta\mathbf{p})^2$ (or the difference-kinetic energy) between the precursor and successor surfaces. The parameter m^2 reappears in a number of contexts dealing with the effective interaction between the reactant and product states, as will be seen below.

The prefactor to the exponential requires more careful treatment than the rather facile methods employed here to obtain the general Marcus' formalism – in particular the treatment by Calef and Wolynes [17] is probably the most thorough, and will be utilized in our further data analysis for the Arrhenius parameters.

The presence of this averaging distribution, together with the prominence of the averaged quantity λ, might lead one to suspect that, at least for the adiabatic case, the rate constant so obtained is really a distribution of effective rates. Now it is important to know why it is indeed the case that the macroscopic rate may be distributed in the adiabatic case, but that the statistical averaging process for the nonequilibrium polarization fluctuations captured in the parameter λ in fact gives one *micro* rate constant, in other words, the statistical nature of the reorganization energy does not 'survive' beyond the calculation of a particular barrier to e.t., and does not conduce to distributing the rate constants at the macro level. The energy-difference function (the barrier is determined by this function) at the intersection is minimized with respect to the centering δfunctional f^*:

$$\langle\delta(E_--m(E_+-E_-))/\delta f^*\rangle = 0; \tag{8a}$$

But the functional derivative in the path-integral formulation is itself equal to (Feynman and Hibbs [18]):

$$(1/k_\mathrm{B}T)\langle[E_--m(E_+-E_-)]\delta H_\mathrm{T}/\delta f^*\rangle, \tag{8b}$$

which, in turn, by virtue of Stokes' theorem, is equal to:

$$(1/k_\mathrm{B}T)\langle[E_--m(E_+-E_-)]H_\mathrm{T}\rangle_{\partial f^*}, \tag{8c}$$

i.e. the difference functional evaluated on the 'boundary' of the centroid defined by f^*. (H_T is the total energy of the system). The second functional integral (9b) then yields $\langle E_-^2-m^2(E_+-E_-)^2\rangle_{\partial f^*}=0$ (since the total energy of the system is given by the total Hamiltonian near the intersection $[E_-+m(E_+-E_-)]f^*$) or $kT\Delta F^*-kTm^2\lambda=0$, which is the same as the determinative equation $\Delta F^*=m^2\lambda$ from Marcus [11], where ΔF^* is the effective Arrhenius barrier height to the e.t. rate process. More accurately,

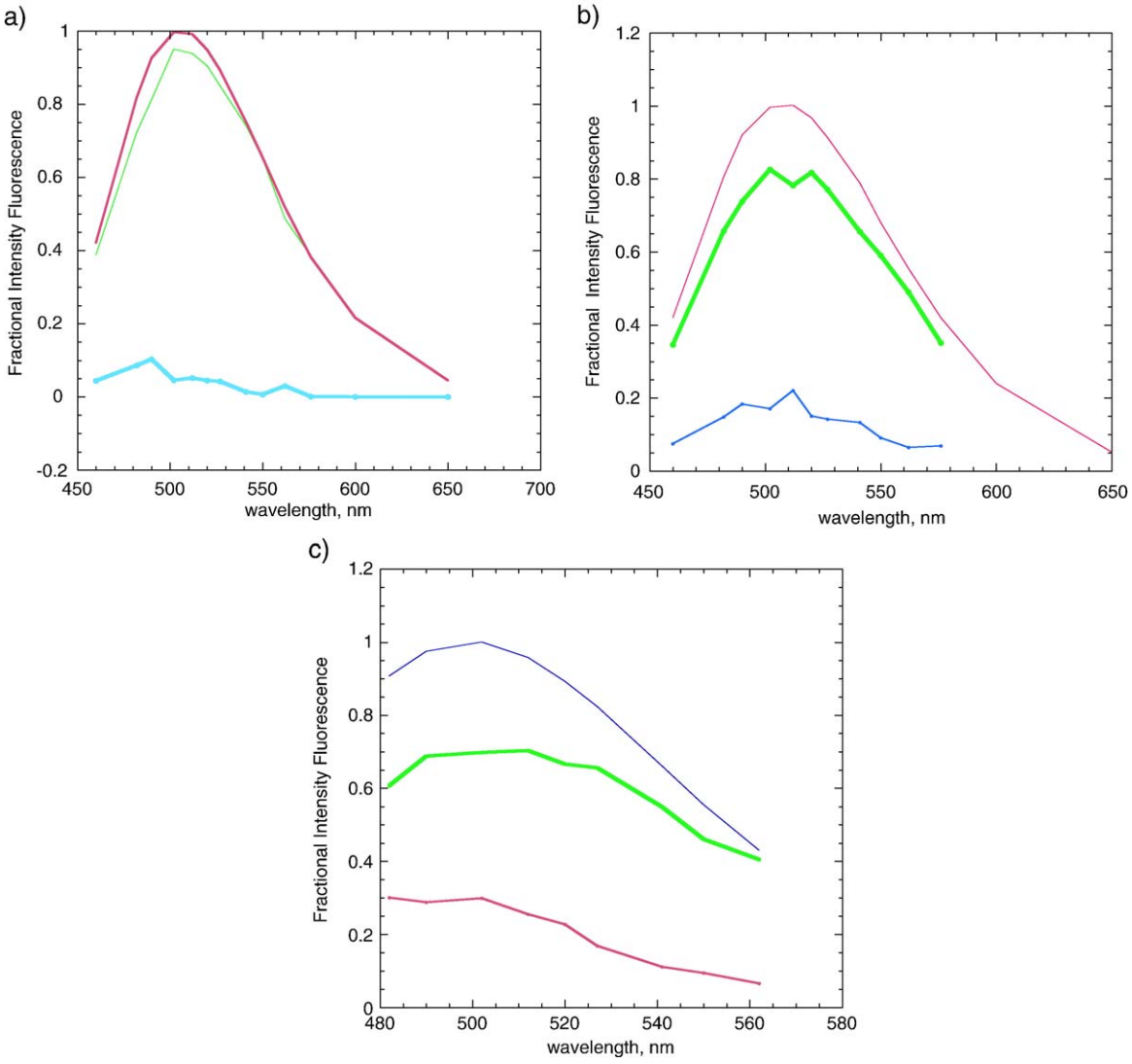

Fig. 7. Species associated spectra of glycerol/H_2O mixtures: (a) 70 vol.% glycerol at 10 °C; b) 70 vol.% at 40 °C; c) 80 vol.% glycerol at 10 °C. Top line with marker is the total fluorescence, thick line is the longer lifetime-component fractional intensity, and thin line is the shorter lifetime component spectrum.

m would be given by $\{1/2+((E_+-E_-)^2+4H_{12}^2)^{1/2}/2(E_+-E_-)\}f^*$.[1] The point, however, is that the *variance* of this barrier energy, or, for that matter, the variance in λ, would be equivalent to a term:

$$(1/k_BT)\langle E_- - m(E_+ - E_-)\rangle_{\partial f^*} \tag{9}$$

which, by virtue of Poincare's lemma, vanishes. Thus the rate for a given configuration of solvent (determined by f^*), which optimizes the transition rate, is a constant. Solvent fluctuations, which generate the electron transfer surface, *do not give rise to* fluctuations of the micro (Marcus) rate constant itself.

There is however, a separation of time scales between the motions of the electron on the surface defining the e.t, that is, the adiabatic surface – the configuration of the solvent which induces f^* – and the motion of these surfaces themselves, the longer times, when they resolve back into their original "diabatic" configuration. If these motions are taken to be independent, then the total macro rate is a product of the probability per unit time of a particular e.t. times the probability of a particular donor–acceptor pair at a distance defined by the acceptor probability distribution, or the product $\chi(\mathbf{r})$, of $g(\mathbf{r})$, and $|\Psi^2|$ the density of the wave function of the newly emerged electron into the solvent – the *solvent-induced polaron*. The rate would then be written as, e.g.

$$R = 4\pi\rho_0 \int \mathrm{d}^3\mathbf{r}\chi(\mathbf{r})k(\mathbf{r}). \tag{10}$$

We use here the radial distribution product of solvent *with* solvent, instead of solvent (acceptor) with solute (donor) not only because we do not have access to the solute–solvent $g(\mathbf{r})$,

[1] This equation arises because of the requirement that the two potential energy surfaces for the 'centered' product and reactant states are not independent, such that the determinant $|(\mathbf{U}+\mathbf{H}_{12})f^* - m\Delta\mathbf{UI}| = 0$.

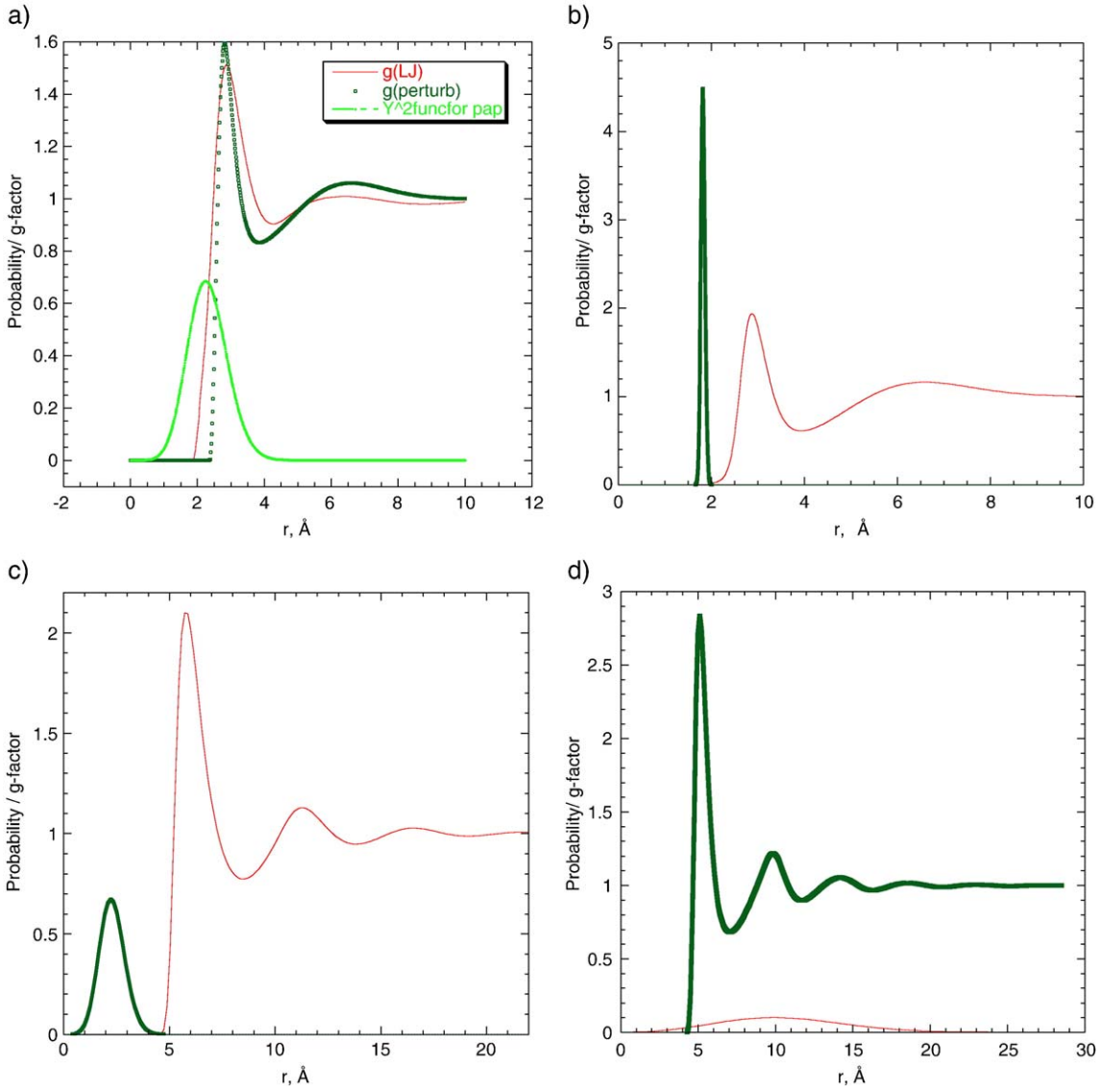

Fig. 8. Solvent oxygen–oxygen pair correlation functions ($g(\mathbf{r})$), LJ-function and perturbed g-function shown, together with derived Morse oscillator density for ethanol (a), for water (b) (g function resembling the experimentally found function for water), for cyclohexanol (c); while in panel (d) the *H.O.* density and $g(\mathbf{r})$ derived for dioxane is displayed. In (c), the perturbed g-function is not noticeably different from the LJ g-function.

but also because the actual successor state, the polaron, subsists at least in part *between* solvent molecules (cf. Fig. 6).

Chandler and coworkers [19–21] developed a theory which encapsulates these effects in the 'excess electron in solvent' model. In their theory, the correlation function arises as a product of a solvent–solvent (site) correlation function, a solvent–electron direct correlation function, and a 'pure' electron response function. What we have done is reason that these combined correlation function are likewise factored into an electron-reacting system correlation function (given by $k(\mathbf{r})$, cf. [3]), an electron–solvent correlation function (polaron wave function), and the solvent–solvent correlation function $g(\mathbf{r})$. Now there are two kinds of cage or boundary of the polaron – i) the solute on one side with the nearest solvent molecule on the other, and ii) between two solvents. These two kinds of cage-boundaries are seen also in two kinds of cage-diffusion and two kinds of cage-breakdown, which are labelled longitudinal and transverse in Fig. 6. Nonetheless we will use just one g-function for both kinds of cage-boundaries. The diffusion of the solvent cage is what we expect controls the Gaussian kinetics of the polaron acceptor state, as the polaron exists in what is essentially a defect in the solvent quasilattice. The concept is similar to the solvent-defect diffusion thought by Glarum to underlie Gaussian dielectric relaxation kinetics [22].

The g-function we utilized is also shown in Fig. 8a for ethanol, in Fig. 8b for water, in Fig. 8c for cyclohexanol, and in Fig. 8d for dioxane. They were generated from Lennard–Jones type g-function obtained from the program implemented online at http://stthd7.pc.uni-koeln.de (with parameters for ethanol of $T^*=kT/\varepsilon_{L-J}=3.18$ and packing fraction $\rho\sigma^3=f_{pack}=0.51$ chosen to resemble the radial distribution function of a L–J potential with a intramolecular O–O distance of 2.85 Å

Table 5
Adiabatic electron transfer from ANS to ROH solvent (25 K)

	ε_0 [a]	ε_∞ [b]	τ_{diel} ($\times 10^{-10}$ s) [c]	$\rho_0\int \Psi^2 g(\mathbf{r}) r^{2}$ [d]	ϕ	f(τ_{diel})	"c" [e]	"$c_{this\ work}$"	A_0 (exp)(s^{-1})	A_0 (calc) [f]	$\Delta F^{\ddagger}$ (exp)
H_2O (soft)	78	4.2/2.1	0.096	–	0.0177	1	1.6	0.216	3.7×10^{9}	4.2×10^{10} [3.2×10^{11}]	~0
EtOH	25	2.2	1.7	0.0046	–	1	1.57	0.581	5.4×10^{8}	2.0×10^{8} [5.3×10^{8}]	1.3
$C_6H_{12}O$	16	2.4	0.02	–	0.0047	0.25	2.05	0.5	7×10^{9}	1.9×10^{9} [7.7×10^{9}]	8.5±8 [g]

[a] ε_0 values from [48].
[b] ε_∞ values for from [45] and [49]; the value of 2.1 more typical of alcoholic solvents is atypical of water, but must be considered at **very** high frequencies (~600 cm^{-1}, cf. [40]). For ethanol and for cyclohexanol ε is taken from [44]).
[c] Dielectric relaxation times from [45] for H_2O; [46] for ethanol; [47] for cyclohexanol.
[d] Morse oscillator density multiplied by the $g(\mathbf{r})$ factors as described in the text. These are integrated and multiplied by the number density.
[e] "c" factor from Calef–Wolynes [17], see text.
[f] Calculated as described in the text, top line is the number calculated using the Calef–Wolynes "c" factor, numbers in square brackets utilize "$c_{this\ work}$".
[g] Average of two fits to $\langle\tau\rangle^{-1}$ and to 'k', the latter being ~19, the former being ~−2 kJ/mol.

assumed to be typical of ethanol or water), which is then *perturbed* by a Morse potential representing the hydrogen bond O–H–O, with a dissociation energy of 6.3 kJ/mol, a stretching frequency of 170 cm^{-1}, and a reduced mass of 8 Da. We employed the following formula:

$$g'(\mathbf{r}) = (g_0(\mathbf{r})-1.00)\exp\left[-4\pi\rho_0\int(V(r)/k_BT)g_0(r)r^2dr\right] + 1.00; \quad (11)$$

with $V(r)$ given by:

$$D[\exp(-2a(r-r_0))-2\exp(-a(r-r_0))] \quad (12)$$

Where 'a' is given by $(2D/M)^{1/2}2\pi\nu$ in cm^{-1} D being the dissociation energy.

The electron is thought to interact with the instantaneous solvent 'lattice' through the solvent–dipole moment. The original polaron model dealt with an ionic crystal lattice. As did Chandler's group [19], we assume that the solvent can be represented by a Drude oscillator. Thus the interaction term of Feynman's theory [18,23] – which, since it ignores the lattice structure, ought to be even more appropriate for a fluid solvent than for a crystal – must be defined rather differently. The coupling parameter α_F of Feynman's theory we now re-define to be:

$$m^2e_0\mu\left(\varepsilon_\infty^{-1}-e_0^{-1}\right)/(\sqrt{2}\hbar 2/M^*), \quad (13)$$

where 'm' is the same quantity defined above in Marcus' theory, M^* is the effective polaron mass, found self-consistently via the dependence of the ratio of the effective polaron mass to the 'bare' electron mass, M^*/M_e, on α_F as determined by Schultz [24], μ is the dipole moment of the solvent, and the ε_∞ is the high frequency dielectric constant (ε_0 being the static dielectric constant). The Drude oscillator associated with each solvent molecule can be thought of as 'stretching' via a force-constant equal to the reciprocal of the static polarizability α_0^{-1}, in response to the electron with an amplitude equal to its root-mean square amplitude as an harmonic oscillator, which also defines the equilibrium separation between the electron and the oscillator (since the excess electron density should be 'centered' on the atom, namely the proton of ROH, where donor molecule electron-dense site has an H-bond to solvent). The polaron wave function was approximated by a Morse oscillator wave function. There are several reasons for this: first, although in its original formulation, the polaron was thought to resemble an harmonic oscillator, there is nothing exclusive about harmonic oscillators – anything which can be done using H.O. wave functions can be done with M.O. (Morse oscillator) wave functions, and more. For example, M.O. wave functions also have well-defined ladder operators [25]. Secondly, the Feynman polaron [23] model obtains a finite binding energy of the electron to the 'lattice', which is, to be rigorous, inconsistent with the assumption of a H.O. wave function, but *is* an intrinsic part of any M.O. model. Lastly, the variational method employed by Feynman utilizes explicitly the properties of quadratic (Gaussian) functionals – and Morse oscillators are in fact quadratic in relative density-differences, instead of displacements, so the underlying variational principle in Feynman's theory should emerge unscathed by our redefinitions.

The Morse parameters are then determined from the following relations: $M^*\omega^2=2Da^2=q^2/\alpha_0$; $D/\hbar\omega=-0.1061\alpha_F^2-2.83$. At this point we have to assume that 'q' is the realized charge on the solvent dipole, or e.g. for ethanol: 1.69×10^{-18} esu-cm/0.975×10^{-8} cm. Then the M.O. probability density, for $n=0$, is written:

$$(a/N)\exp[-2K(\exp(-a(r-r_0)))]\exp[-(2K-1)a(r-r_0)], \quad (14)$$

where $2K=(2M^*D)^{1/2}/a\hbar=2D/\hbar\omega$, and N is a normalization factor [26].

Fig. 8 also shows normalized M.O. densities with the g-functions discussed above. We note at this point that we take the polaron boundary to be outside of the ANS molecule, in fact it is located at the same distance as the *proton* of an ROH solvent, supposed to be hydrogen bonded to a site on the ANS, in other words, the r_{eq} for the Morse function is taken to be 1.8 Å [27] for all ROH-type solvents.

When a polaron wave function is broad, of low M^*/M_e ratio, coinciding with a small α_F, which usually also implies a large polarizability, small D', and/or small ε_0, it is generally referred to as 'soft', and if the situation is reversed, it is called a 'hard' polaron.

The purpose of the theoretical development we have presented here is to enable us to predict the macroscopically measured rates, or at least the Arrhenius prefactor from the observed activation energy (in principle even predict the $\Delta E_A^{\ddagger}$), and moreover, to predict the observed lifetime distribution *widths* from fundamental properties of the molecules con-

cerned. To return to the macroscopic Eq. (11): the expression for 'k' given by Calef and Wolynes [17][2] is:

$$k(\mathbf{r}) = (\varepsilon_0/\varepsilon_\infty \tau_d)(\mathbf{f}(\tau_{\rm rot})/c)\exp(-\Delta F^*/k_{\rm B}T) \qquad (15a)$$

(although the **r** dependence is small) where there are two cases, called A and B, respectively, wherein, for case A, the electronic coupling Hamiltonian H_{12} is small relative to $k_{\rm B}T$, and case B when they are comparable. The factor 'c' is equal to:

$$(4k_{\rm B}T\lambda)^{1/2}\left\{|\Delta F^0 + \lambda|^{-1} + |(\Delta F^0 - \lambda)|^{-1}\right\} \qquad (15b)$$

for case A, and:

$$2\pi\left[\left|\left\{(\lambda^2 - \Delta F^{0\ 2})^{3/2}/8\lambda^2 H_{12}\right\} - 1\right|\right]^{-1/2} \qquad (15c)$$

for case B.

The factor $\mathbf{f}(\tau_{\rm rot})$ is very close to 1.00 for many solvents, and is almost certainly so for protein matrices. We suppose that case A is more relevant to us.

3.1.2. Evaluation of rate constant expressions

In Table 3 we present the various contributions to the free energy of reaction $\Delta F^{0\prime}$. For the site-solvation, the summed energies of the charge–transfer site solvation calculated in Part II in this series were used, except that it is expected that there is only 1/2 the amount of charge distributed about the ANS molecule (that is, the earlier contribution gave the sum of an electron charge excess in the naphthalene plus a deficiency charge in aniline, so that the total solvation energy here is half the total of the previous paper). We also assume that the charge–solvent dipole interaction contributes most to the site–solvation energy for both ethanol and water. While the dipole moment of ethanol is 1.69 D, compared with 1.84 D for water, ethanol has a much larger polarizability, so the net effect should be roughly similar. With a generous uncertainty, we predict -90 ± 40 kJ/mol of site–solvation energy in Table 3. To evaluate the various terms in the Arrhenius-type expressions for the rate constant of (17a,b), we employ the temperature derivatives given in Appendix B. For water, we calculated the expected Born hydration energy both of an electron surrounded by 4 waters (a hard polaron possibly) and one surrounded by a tetrahedron of tetrahedrally coordinated waters, 12 in all, similar to what we fit in the Introduction, and perhaps indicative of a 'soft' polaron. As it turns out (see below) the actual polaron in water is probably harder yet than the assumed structures we used here, being confined to the nearest available water site (Fig. 8b).

For convenience the temperature derivatives are collected into Table 4. The table also displays temperature derivatives of parameters on which the theory we employ depends. To fit the observed Arrhenius dependence we require their values, yet we require the fitted activation energy to determine these very values (e.g. we need 'm' or λ, either of which we can only obtain from the expression for ΔF^*, where $\Delta F^* = (\Delta F^{0\prime} + \lambda)^2/4\lambda$, but we can only obtain ΔF^* after factoring out ΔS^*, which requires an explicit form of the polaron wave function, which in turn requires a value for λ). The values therefore are obtained iteratively.

To illustrate: for ethanol the slope of dln(Rate)/d1000/T was found to be -0.52. This must equal (cf. Appendix B and Table 4) the sum:

$$-0.52 = 0.126 + .412 - 2.47 - {\rm dln}c/{\rm d}1000/T - T\Delta S^*/1000 - w^{\rm R}/R - .00375 - \Delta F^*, \text{ and}$$

where

$$\Delta S^* = -R{\rm ln}Z_{\rm trans}; \qquad Z_{\rm trans} = (V_{\rm pol}/V_{e^-})\Lambda^3_{e^-}/\Lambda^3_{\rm pol} \qquad (16a,b)$$

wherein the 'volume' of the bound electron occupies $V_{\rm e}$ is roughly the volume of the naphthalene, and the volume of the polaron, $V_{\rm pol}$ is $(2\pi)^{1/2}\sigma^3$ (since the density looks nearly Gaussian), the de Broglie wavelength of the polaron $\Lambda_{\rm pol}$ is $m(2M^*kT)^{1/2}/\hbar$ and the de Broglie wavelength of the electron as bound is $(2_{\rm mel}V_{\rm bind})^{1/2}/\hbar$ and lastly where $V_{\rm bind} = I_{\rm p} - h\nu$ for which we already have values listed in Table 3. Now, at first, we can consider the Calef–Wolynes model for "c" and its temperature derivative, as given in Appendix B. And we can also assume that $\lambda \approx 50$ kJ/mol and $m \approx .45$ to derive the polaron properties for ethanol. The value of $-w^{\rm R}/R$ is dln(**r**)/d$(1/T)$ and equals roughly 0.12. From these assumptions we obtain $\Delta F^* = 6.4$ kJ/mol, $\lambda = 33$ kJ/mol, $m = \sqrt{(\Delta F^*/\lambda)} = 0.44$. Using further iterations and taking (since the value for "$c_{\rm this\ work}$" seems to fit better) $-1/T$ for dln$c$/dT, we obtain values presented in Tables 4 and 5 which are self-consistent, namely $\Delta F^* = 5.2$ kJ/mol, $\lambda = 35$ kJ/mol, so that $m = 0.39$. A similar procedure is employed for the case of H_2O and cyclohexanol.

The values obtained for the Arrhenius prefactor in Table 5 are compared there with experiment. Only in the case of water is the agreement less than impressive, and if the final acceptor state is a water proton the fully adiabatic formalism may not be appropriate, as we shall discuss presently.

As we saw, in the case of water (Fig. 8b), the polaron density appears in a region from which the nearest neighbor solvent *center* is excluded. In ethanol, we have supposed that the polaron subsists between two solvent molecules (at least). The conjoint probability function (polaron + cage) given by $\int|\Psi|^2 g(\mathbf{r})r^2\rho_{\rm sol}{\rm d}r$ for water is very small, and probably not relevant to this case. If the polaron is, instead, inside this nearest solvent molecule, not *between* solvent molecules in the first solvation sheath, this probability should instead be written as $\rho_{\rm sol}V_{\rm pol}f_{\rm pack}$

[2] The "c" factor is derived from a calculation of the 'mean first passage time' through the barrier region, or, the expected time at which the donor and acceptor diabatic surfaces irreversibly separate. Since the electrostatic potential in this region is given by $-m^2\lambda/{\rm e}_0$ the potential is very nearly an inverted parabola in our dimensionless variable 'm'. This region thus has an effective curvature of $-\lambda$. However the boundary of this reactive region is defined by critical points where the curvature goes through zero (and it is positive, defining a potential energy well, on either side of this zone). Then, if, as Calef and Wolynes do, we call the 'diffusion constant' of this region $\varepsilon_0/(\varepsilon_\infty\tau_{\rm diel})$, we find, instead, that $\tau_{\rm mfp} = \tau_{\rm diel}\int_x^{x_{\rm b}}\exp(+\kappa y^2/2kT){\rm d}y\int_{x_{\rm a}}^{y}\exp(-\kappa z^2/2kT){\rm d}z$ cf. Zwanzig [3] with our special $\kappa = -\lambda/2$ near the peak of 'x'. As per our discussion above, at $x_{\rm a}$ and $x_{\rm b}$, $\kappa \approx 0$, and $x^2 = (\Delta F^0 + \lambda)^2/\lambda^2$ near the peak. Thus we obtain a "c" factor of $(4\pi kT/\lambda)|\exp(-((\Delta F^0 + \lambda)^2/8kT\lambda)) - 1|$ which is distinct from that given by Calef and Wolynes [17], and which we report in Table 5 as "$c_{\rm this\ work}$".

as we have done in Table 5, representing the probability of a solvent molecule being present at the radius of the polaron (f_{pack} substituting here for the effective 'g' factor). Both the compactness or hardness of the water polaron and its position, as well as its mass, suggest that the electron in H_2O may be unstable relative to an $H^{\cdot}$, proton attached, state.

Even by employing different values for the electron affinity, say that of a single water, about 24 kJ/mol [28], in Table 3, we cannot noticeably decrease the polaron mass for water, rather the reverse. The large mass of the water polaron can be traced to two features of the solvent – 1) its low polarizability, together with 2) the (usual) large reorganization energy in water, and neither of these phenomena are very sensitive to changes in $\Delta F^{0\prime}$.

Our formula for the rate yields a much higher value than is observed for the Arrhenius prefactor. The H_2O/D_2O ratio of the lifetimes we found in Kirk et al. [15] was 2.48. Since the effective activation energies are near zero, these are also very nearly the reciprocal prefactors. Such an isotope effect is larger than typical for solvent isotope effects (the τ_{diel} ratio being about 1.13), but smaller than many typical Franck–Condon factor ratios for H vs. D or values of *primary* hydrogen isotope effects (~2–10), arising from mass ratio effects in partition functions in the transition state. We speculate that the rate of e.t. may be 'mixed' – part adiabatic and part nonadiabatic. The system progress adiabatically up to a reactive zone, but the actual electron transfer cannot occur over a single surface, the electron must jump, while in this zone, between still disconnected surfaces. The adiabatic rate part of the ensuing total rate might still have a factor $\varepsilon_0/\tau_{diel}\varepsilon_\infty$, and thus be limited by a factor of $\sim 3\times 10^{12}$ s^{-1}; this is then to be multiplied by a term $\sim\langle H_{12}\rangle^2/(\sqrt{2\pi})kT\lambda$ which would also have a Franck–Condon factor for the product $H^{\bullet}$ –OH (vs. $D^{\bullet}$ –OD).

An interesting observation by Ebbeson and Ghiron [28] that the solvated electron only appears after a '2-photon process' during ANS quenching in water, may have an explanation within these considerations. Their data showed that the onset of the typically solvated electron absorption spectrum follows a quadratic function of the laser intensity incident upon ANS in water, at roughly 362 nm. If the product state in water were indeed H°, an electron attached to a proton from a nearby water molecule, then we might expect that dissociation from this state to the solvated electron state requires the same energy as from a $n=2$ (presumably the $n=1$ shell is already filled) Rydberg orbital on H. The resulting orbital energy would require about 365 nm light to dissociate.

We note for ethanol/water mixtures at 90 mol% and 50 mol% EtOH that the distribution of lifetimes fitting *fails*, i.e. that the observed lifetimes are sums of two single exponentials. We were attempting to find the first appearance of the effect of *one* water molecule, ostensibly breaking an hypothetical inner-salt in the excited state between the N–H and the SO_3 (which facilitates the orthogonal disposition of the rings observed in low polarity solvents, cf. Part V in this series), and leading to reduced lifetime/narrow distribution/two single exponential lifetimes. Needless to say, we did not observe such a 'transition'. It is possible that it may take place in a fairly narrow range of water content. It is also clear that, whereas in 90% EtOH, the shorter component comprises roughly 10% of the decay, nonetheless at 50% it is not, even roughly, 50% of the decay. That is, the two 'species' are not the result of a slow equilibrium of inner solvation spheres between 'water-rich' vs. 'ethanol-rich'. Table 2 also gives decay data as a function of emission wavelength, which mirrors some results we obtained with glycerol/water mixtures. It is found that the shorter decay seems to emit generally more to the blue of the longer decay, despite the fact that in pure water the decay is shorter than in ethanol, yet the emission is to the *red* of that in ethanol. We will discuss this aspect more fully with respect to the glycerol/water solution data.

The scenario we envision for ethanol/water mixtures, then, is that the reorganization energy and ΔF^0 values smoothly progress toward the pure ethanol or pure water values from either direction, but that, whereas in pure ethanol a relatively freely diffusing polaron is the successor state, as the water content increases, ensuing structural disorder *localizes* the polaron (Anderson localization [29]), preventing diffusion and narrowing the lifetime distribution.

At 90 mol% ethanol, there are already two distinct rotamer states, each generating a narrow lifetime: as we imagine the situation – 1) the 'high phenyl' characteristic of nonaqueous solutions (cf. Part V in this series), giving way with increasing water content to the 2) 'intermediate phenyl' rotamer. These would constitute the two 'states' from which decay originates. As we mention, it is conceivable the two rotamers differ in the presence of a 'bridging' water molecule, which is why the 'high' rotamer predominates at lower water concentrations and in nonprotic solvents. The position of the phenyl group, in this view, serves to 'gate' water molecules at bay region of naphthalene and the SO_3/NH 'site'.

The requirement we observed at the outset of this paper for ~13 waters implies that a large cluster of water is necessary for the water-like rate to appear, so that the 'gating' by the phenyl group is rather effective at excluding water until there already is a large amount of water at hand. Another possibility, though, is that the polaron-in-water, confined as we imagine it to be to the nearest proton, or as we argue, possibly even *unstable* relative to an H°, needs to be created in an 'H' defect zone in the hydrogen bonded solvent: a place where the H– –O– – –H– –O chain is 'broken', and one localizes an O– –H H– –O (an H-bond defect) instead. Such a defect might require as many as 13 waters to form.

For cyclohexanol electrochemistry, we assume that at the distance to the center of the cyclohexanol molecules surrounding ANS (approximately 8.75 Å), the polarizability tensor responds to an electric field which is essentially the same for all surrounding cyclohexanol molecules; that is, there is no specific association of any cyclohexanol molecule to any one particular site on ANS. We assume that of the 11 molecules which could fit about ANS at that distance, two are excluded by the anilino group and one is excluded from the nearest neighbor packing by the orientation of the OH group *toward* the naphthalene. The field at a distance **r** from a uniformly charged (of charge q) sphere of radius **R** is then approximated by the series:

$$\mathbf{E} = q\{-1/r^2 - 2R/r^4 + 5/16R^4/r^6 - 53/70R^6/r^8 + \cdots\}$$

We calculate the value of $-1/2\alpha_0\mathbf{E}$ and multiply by 8, with $\alpha_0=11.56$ Å the polarizability of cyclohexanol. This contribution, ~23 kJ/mol, is not a small fraction of the dipole–field interaction for cyclohexanol (in contrast to the case with ethanol or water), which we assumed in Table 3 to be about 40 kJ/mol.

We also chose a value for kT/ε_{L-J} for cyclohexanol of 1.11 [30]. Again we perturb the *g*-function obtained from the site http://stthd7.pc.uni-koeln.de/ with these input parameters as per Eq. (11) and obtain the new $g'(\mathbf{r})$ as displayed (it does not at this scale differ markedly from the original *g*-function). The value for '*m*' we obtain is roughly 0.45 and the resulting polaron density is shown in Fig. 8c. The calculation of the expected Arrhenius prefactors is hampered by the lack of reliable data for dioxane. For example, Antony and Smyth [31] report a τ^{-1} of 6.06×10^{10} for a solution of $CHCl_3$ in dioxane at infinite dilution. Taking this to represent dioxane itself, and assuming that λ is roughly 7.3 kJ/mol (from Eq. (6) assuming 4.75 Å for the diameter of dioxane), we estimate $\Delta F^{0\prime}$ as ~+11 kJ/mol. The dipole moment vanishes for the 'chair' configuration. And though the 'boat' may have a larger dipole moment, the factor of $1/\varepsilon_\infty-1/\varepsilon_0$ is still very small. Thus the α_F is nearly zero and the mass ratio is 1.00. Put another way, the solvent polaron per se is not applicable in pure dioxane. However we do not think the ejected electron is altogether free, either. If the electron sees an effective force constant due to the polarizability ($1/\alpha_0$) of the solvent, then it can still be in a bound state. If we now write a harmonic oscillator density, with $|\Psi|^2=\exp(-m\omega x^2/\hbar)=\exp(-e_0x^2\sqrt{\{[1/\varepsilon_\infty-1/\varepsilon_0]m_{el}/\alpha\}}/\hbar)$ we have a broad but not infinite ranged function (Fig. 8d). Even so, we calculate using our "*c*-factor" an Arrhenius prefactor of 2.1×10^{10} s^{-1} (using the Calef–Wolynes "*c*" factor it is $>1\times10^{11}$ s^{-1}), which agrees poorly with the observed value (2.5×10^9 s^{-1}) – although this may well be due to the wrong value for τ_{diel}, and possibly a too-high value for λ.

For all the pure solvents, the uncertainty in $\Delta F^{0\prime}$ and in λ produces ~50% uncertainty in calculated rate. In view of the uncertainties involved and the number of assumptions made, our general agreement with the data is good.

3.2. The diffusion of the polaron

The 'macro' rate, from (12) is, again: $R=4\pi\rho_0\int d^3\mathbf{r}'|\Psi(\mathbf{r}'-\mathbf{r}_{eq})|^2g(\mathbf{r}_0)k(\mathbf{r})$ or $R=4\pi\rho_0\int d^3\mathbf{r}|\Psi(\mathbf{r}-\mathbf{r}_{eq})|^2g(\mathbf{r})k(\mathbf{r})$ where $\mathbf{r}'=\mathbf{r}-\mathbf{r}_0$ with the position of the electron being $\mathbf{r}$ and the position of solvent being $\mathbf{r}_0$ with the ANS at the origin. To reiterate, we have assumed for simplicity that we can use the same *g*-function for solvent–solvent separations and solvent–ANS separation, so effectively there is no difference between the formulas.

The *generating function* [32] for the rate-distribution is the Laplace transform of this expression, since the coefficients in the Taylor expansion of the generating function are the *moments* of the distribution. Then, as can be readily ascertained, the width of the distribution in rate-space, $\sigma_k=\sqrt{|a_2-a_1^2|}$, where a_i is defined such that $P(t)=\int dkP(k)e^{-kt}$ and $P(t)=\sum_n(-1)^na_it^{-n}=\sum_nt^nP(t)/dt^n/n!$. For the rate distribution equation, we notice that, in a sense, we already have an extra time derivative (because it is a rate equation) and for the a_i we have to identify terms involving the same order of '*t*'. Thus the general probability distribution $P(t)$ in time as we defined above is the 'rate distribution' $R(t)=\int\int dk4\pi\rho_0k(r)\chi(\mathbf{r})r^2dre^{-kt}=-\int\int dk4\pi\rho_0)\chi(\mathbf{r})r^2drd(e^{-kt})/dt$. So the 'first derivative' must be implicitly multiplied by '*t*' to obtain *a* (which would then be in proper units of t^{-1}), and similarly with the second derivative. The first derivative of the integrand to the above Laplace transform is $-\langle k\partial\chi/\partial t\rangle+\langle\chi k^2\rangle$, and the second derivative is $-\langle k\partial^2\chi/\partial t^2\rangle+2\langle k^2\partial\chi/\partial t\rangle-\langle\chi k^3\rangle$. We utilize here the bracket notation to represent the averaging integral over '*r*', as defined above. We are interested in times such that 't_0' ~ τ_0: then $|a_2-a_1^2|=2\langle k_0^2d\chi/dt\rangle\tau_0+k_0^2\tau_0^2\langle d\chi/dt\rangle$, and since $k_0\tau_0=1$, we obtain:

$$\sigma_k=|2\langle k_0d\chi/dt\rangle+\langle\partial\chi/\partial t\rangle^2|^{1/2}. \tag{17}$$

Our model for $d\chi/dt$ is simply that of a diffusion reaction. The solution for a diffusion reaction without drift:

$$d\chi/dt=-D/2\partial^2\chi/\partial r'^2 \tag{18}$$

yields a form which greatly resembles a Gaussian (*D* here being the diffusion constant of the solvent). We take the second term in (18) since the fluctuation of $\langle d\chi/dt\rangle$ will generally cause it to vanish.

The second derivative of r'^2 times the function in Fig. 8a, when integrated over r', yields 0.65 Å. The number density of pure ethanol is 0.0103 molecules/Å^3. The diffusion constant of water in ethanol (or ethanol in water, or ethanol in ethanol, etc.) is roughly 120 Å^2/ns. Given the actual values of the lifetime, we can calculate the expected rate 'width' to be $\sim4.3\times10^8$ s^{-1} from (18).

In order to compare this value to the observed lifetime width, it would be most preferable to accomplish the decay fitting in '*k*' space. Unfortunately, the 'Globals' program we employed seems to be unable to fit distributed decay functions in reciprocal time, at least as ascertained by the frequency with which the routine 'crashes'. The time–Gaussian distribution is given by:

$$R(t)=(2\pi)^{-1/2}\sigma_\tau^{-1}\exp(-(\tau-\tau_0)^2/2\sigma_\tau^2) \tag{19}$$

'Inverting' a Gaussian generally gives rise to an effectively wider distribution than we have implied above. One still recovers a Gaussian in rate space if $\sigma_t/\tau_0\sim0.3$ or less. A useful interpolating formula for the rate–space width is:

$$\sigma_k\sim\sigma_t/\tau_0^2(1+\exp(\sigma_t/\tau_0)+\exp((\sigma_t/\tau_0)^2))/3. \tag{20}$$

Using this formula, we obtain a σ_k of about 1.3×10^8 s^{-1}, about one-third the value we calculated above.

In water the calculation is not useful since our model of the polaron there is flawed. In cyclohexanol, we employed a substitute for our original formula for the $\chi(\mathbf{r})$ integral. To be consistent, we now use just the derivative of a Gaussian (since the density looks close to a Gaussian distribution), evaluated between + and − σ i.e. $2e^{-1/2}(2\sigma+R)/\sigma^2=\langle d^2\chi/dr^2\rangle$; we then multiply by $(D/2)\rho_0f_{pack}$ for cyclohexanol, assuming $D\approx50$ Å^2/ns, we thus obtain an expected σ_k of $\sim3\times10^8$ s^{-1} to be compared with the 'observed' rate width of $\sim1\times10^8$ s^{-1}. If we

attempt the same calculation for water, we obtain a time width of about 10^{-11} s, which is certainly consistent with the discrete appearance of the decay in water.

Because the density for dioxane is long-ranged, the pair correlation function (it is not obvious that we need oxygen–oxygen pairs), is probably not particularly informative – the polaron subsists in nearly disordered solvent. In such case, instead of the lifetime distribution being fairly large, it is found, somewhat counterintuitively, that the diffusion rate effectively *vanishes* (the Anderson localization effect again – see Anderson [29]). In the Anderson process, an electron localizes in a region where a number of weak lattice 'defects' happen to congregate. Either with a disordered environment or with a broad 'soft' polaron, diffusion is suppressed [33]. Anderson localization can actually be explained even more simply: as long as $g(\mathbf{r})$ is precisely 1.00, as in bulk liquid, then, since the diffusion equation asks for the difference 'slope' of the polaron density and that density is itself a symmetric function, the average value of $d\chi/dt$ is zero. On the other hand, even with a rapidly varying $g(\mathbf{r})$, such as in a 'hard' lattice like an ionic crystal, as long as the polaron is quite spread out, this slope is averaged over several oscillations in $g(\mathbf{r})$ and so it once again vanishes. The polaron model thus accommodates both the 'diffusion width' of lifetime distributions seen in nearly pure ROH solvents and the disappearance of the said width in mixed, disordered, solvent systems.

4. Inhomogeneous mixtures – glycerol/water

In Fig. 7 we plotted the species associated spectra (SAS) we recovered for our glycerol/water mixtures. What we see is that at 70% and even more in 80% glycerol at 10 °C there are clearly two 'kinds' of emissive species. The shorter emission lifetime is associated with the bluer, more 'alcohol-like' shifted species, and the longer with the redder, more 'water-like' emission. There is also more of the bluer species at 80% glycerol. At higher temperature the difference in SAS nearly vanishes. Spectral shifts are determined mostly by the short range, nearest neighbor, character of the solvent [34,35].

If nearby solvent dipoles can reorient, they produce greater Stokes shifts than when they cannot. In nonpolar solvents, only the polarizability contributes to Stokes shifts [34]. In electronic transitions with substantial charge–transfer character, the Stokes shift is also proportional to the solvent reorganization energy λ of electron–transfer processes [36]. As we have seen, such a correlation is still present in ANS/ROH solvent systems, although it is not quantitative.

The bluer species we assert does in fact represent the presence of glycerol in the first coordination sphere, nearest to the excited state dipole. And, as in the case of alcohols, there is markedly less solvent dipolar reorientation than when only water is present. Perhaps the presence of even one glycerol can severely retard this reorientation among such 1st sphere waters as may be present. If, moreover, the 480-emitting species has an occluded bay region resulting from the 'high phenyl' conformation, typical of less polar solutions (V), then any water present may well be isolated, not part of an extended Hydrogen-bond network and therefore not likely to engage in the typical reorientation of watery solutions, and not producing the Stokes shift typical of water, The 530 nm-centered emission may involve the 'low' phenyl rotamer, and contrariwise may possess an intact H-bond network of ROH to bring about a more water-like Stokes shift. Why, then, does it quench at rates closer to those found in ethanol rather than water?

Table 6
Polaron parameters

Solvent	α_F	M^*/M_e	D (kJ/mol)	$2K$	a (Å^{-1})	Λ ratio (bd/pol)
Ethanol	10.76	168	188	30.2	0.31	0.1175
H_2O (hard)	>26	>25,000				0.562
H_2O (soft)	16.55	1436	278	67	2.92	0.276
Cyclohexanol	12.6	377	106	39.4	0.264	1.01
Dioxane	0	1	0	0	0.188	

The Λ ratio is the ratio of the de Broglie wavelengths of the polaron to that of the bound electron, as described in the text. This ratio is used to generate ΔS^* values, as described in the text. 'Hard' vs. 'soft' values for water result from assuming the electrochemistry values for a 4-water and 12-water cluster, respectively. For dioxane 'a' is the reciprocal width constant for a harmonic oscillator density corresponding to a Drude oscillator within the solvent with slope $=(e^2/\alpha)[1/\varepsilon - 1/\varepsilon]$.

Presumably the effective polarizability of Drude oscillators is markedly more like solvent alcohol than solvent water, and the subsequent polaron is more long-ranged and ethanol-like. Thus at 80 vol.%, there is even more of the short decay species than at 70% (although it decays slightly slower than in 70%), because there is a greater chance for the high rotamer configuration (a water present in the bay region stabilizes the 'low-phenyl' rotamer, in this view). The reverse question, why does the blue emitting species decay with a rate more nearly resembling water than ethanol?, may be more interesting. We assert that the 'high phenyl' rotamer excludes water from the bay region near the sulfo.

This rotamer then emits as in ROH solvent, with a peak ~460–500 nm. The 'hardness' of the polaron, how localized it is seems to be mostly a function of the 'm' value requisite, and hence proportional to the value of $\lambda(\sqrt{(\Delta F^*/\lambda)}$, and to a lesser extent of the reciprocal polarizability. It would seem in glycerol water solutions near 50:50 mol% and 10 °C, that the blue-emitting species would possess either a *larger* value of the reorganization energy than the red-emitting r species, contrary to expectation (i.e. $\lambda \approx$ Stokes shift), or else the solvent configuration is more *frozen* and the solvent is effectively less polarizable than in the 'low phenyl' rotamer. The Anderson localization can also be seen in these experiments. Because of the disorder of the mixture, as well as the viscosity, each kind of polaron is effectively trapped, and the decays are discrete, not broad.

Our values for the width of the lifetime distribution for ethanol and cyclohexanol are both about three times the observed value. As we have already supposed the polaron subsists between solvent-pairs, or between solute and 1st solvent, it is conceivable that using the macroscopic diffusion constant for the solvents in 3 dimensions overestimates the local diffusion rate, which is effectively 1 dimensional. If so, our agreement with the data is very good.

Nodelman and Martin [37], presented a mechanical model for caging effects in aqueous alcoholic solutions and other mixed

solvents, which was able to reproduce an intriguing feature of cage kinetics occurring at 80–90% H_2O (and also ~90% alcohol) in such systems. Namely, from 0.2 mole fraction H_2O to ~0.8 H_2O there appears to be a monotonic decrease in the ratio of methane/ethane production in azomethane decomposition reactions. But in the regions of interest there is a reversal of this tendency, so that at ~90% water there is the global minimum of this ratio, and at 80% alcohol the global maximum occurs. This ratio reflects the tendency of caged photoproduct to abstract a proton from the 'cage', vs. for two such cages to collide, or for the two methyl photoproducts in one cage to react. Thus, the ratio decreases as the cage lifetime increases, which directly reflects the 'longitudinal' vs. transverse decay time in the cage. Nodelman and Martin's model succeeded in reproducing this behavior where simpler expressions involving e.g. the viscosity alone failed. Their fit parameter however, is a rather complicated function of the cohesive energy density, the internal pressure and the ratio of activation enthalpies for viscous flow at constant volume to that at constant pressure, together with a 'lattice' correction. While basing their analysis on a diffusion model, the quantities employed are macroscopic in nature and must be determined empirically, yet this is, after all, an attempt to explain *micro*scopic phenomena. Furthermore, the justification for the particular quantities employed and their relation to each other seems rather *ad hoc*. Nonetheless it is the agreement with the observed kinetics is striking, and it remains the most successful model of diffusion and cage effects in mixed solvents to date. Our 'polaron' model, on the other hand, could be determined entirely from 'first' principles if a sufficiently powerful computer simulation of water+alcohol mixtures could be found to generate the $g(\mathbf{r})$ [38]. Failing that, $g(\mathbf{r})$ could still be determined empirically from X-ray and neutron scattering experiments. The other quantities could be determined the same way. Additionally however, one would require first principles values for λ or 'm', not merely empirically derived ones. While there has been some progress in this area (cf. [39]), much more could be done in the future on this difficult problem in nonequilibrium quantum–electrodynamical statistical mechanics.

The polaron e.t. model we have employed seems to have promise to provide an accurate microscopic picture of caged transient electrons in solvents. Even where the model seems to fail, e.g. in H_2O, it delivers nonetheless interesting suggestions about some aspects of the decay process – possible 'localization' at a proton, the possible origin of the observed isotope effect, and the absence of decay distributions.

Acknowledgement

This work was supported by NIH grant GM34847 to Franklyn G. Prendergast, in whose laboratory this work was performed.

Appendix A

For the adiabatic case, then, the solvent sees a standing wave in the electron field to which it must try to adjust, reaching a compromise between the two phases of the standing wave ('in' vs. 'out') by which the effective barrier to e.t. is erected. We can start by writing out the number of electrons that appear on acceptor sites up to time t', as a direct sum

$$N(t') = \sum_{\mathbf{x}_1 \in \mathbf{X}_1} \sum_{\mathbf{x}' \in \mathbf{X}'} \int d\mathbf{x}' \Delta\delta(\mathbf{x}_1 - \mathbf{x}') \tag{A1a}$$

for a product trap region $\mathbf{X}'$ and a set of paths or trajectories of single electrons between the two centers $\mathbf{X}_1$. The integral over the delta function sets up a single 'count' of a trajectory going into the product trap. Now, taking cognizance of the fact that each path has a characteristic time, and introducing an integral over paths, we rewrite (1a) in terms of integrals:

$$N(t') = \int_0^{t'} dt_1 \int_{X_0}^{\mathbf{x}'} d\mathbf{X}_1 \int_{\mathbf{X}'} d^3\mathbf{x}'' \, \Delta\delta^3(\mathbf{x}_1 - \mathbf{x}'') \tag{A1b}$$

where each delta-function is now generated in terms of the Green's function (cf. Greiner and Reinhardt [40]; also Simon and Jorgenson [41], for the particular choice of Green's function) or propagator $G(\mathbf{x}', t; \mathbf{x}_1, t_1)$ such that

$$\Delta\delta^3(\mathbf{x}_1 - \mathbf{x}'') = \int_{\mathbf{x}_0}^{\mathbf{x}'} d^3\mathbf{x} G^*(\mathbf{x}, t; \mathbf{x}'', t_1) G(\mathbf{x}_1, t_1; \mathbf{x}, t) \tag{A1c}$$

Proceeding from right to left and inserting (1c) into (1b), we have the integral over each whole path $\mathbf{x}_1$ of the propagator–product from a point in the reactants ($\mathbf{x}_0$) to a typical point in the products space ($\mathbf{x}'$), an integral of this quantity over the dummy variable $\mathbf{x}'' \in \mathbf{X}'$, to obtain one 'count', an integral over all such paths from $\mathbf{X}_0$ to $\mathbf{X}'$, and lastly an integral over the arbitrary path–times t_1 up to the time t'.

Then write:

$$\begin{aligned} G(\mathbf{x}_1, t_1; \mathbf{x}, t) \equiv G(t_1, t) &= -i \sum_n \left\langle \mathbf{0}^N, \mathbf{x}' | \mathbf{d} \exp(-i/\hbar \mathsf{H}(t_1 - t)) | \mathbf{n}^{N+1} \right\rangle \\ &\quad \left\langle \mathbf{n}^{N+1} | \mathbf{a}\dagger \exp(i/\hbar \mathsf{H}(t_1 - t)) | \mathbf{0}^N, \mathbf{x}_0 \right\rangle \\ G^*(t, t_1) &= i \sum_n \left\langle \mathbf{0}^N, \mathbf{x}_0 | \mathbf{d}\dagger \exp(i/\hbar \mathsf{H}(t_1 - t)) | \mathbf{n}^{N-1} \right\rangle \\ &\quad \left\langle \mathbf{n}^{N-1} | \mathbf{a} \exp(-i/\hbar \mathsf{H}(t_1 - t)) | \mathbf{0}^N, \mathbf{x}' \right\rangle \end{aligned} \tag{A2a, b}$$

We have interposed a complete set of states $|\mathbf{n}\rangle$ between the initial $|\mathbf{0}, \mathbf{x}_0\rangle$ and final $|\mathbf{0}, \mathbf{x}'\rangle$ configuration to take account of the time-dependence, and we have introduced creation/annihilation operators for the *donor* $\mathbf{d}^\dagger(\mathbf{d})$ and *acceptor* $\mathbf{a}^\dagger(\mathbf{a})$ sites. Note that, since the propagators now do not begin and end in the same state, the product $G^*(t,t_1)G(t_1,t)$ does not in fact equal *precisely* the delta function as it is given, unlike the usual case, but where the Green's propagators disagree in their arguments, since the two expansions are over, respectively, one more and one less electron than is present in the original donor +acceptor system (N), there is now an oscillatory component. Our plan is to consider the Fourier time transform of the previous equation, so as to obtain a delta function in energy, not about zero, but about the 'remainder' between the two propagators. One sees readily that this 'delta function' will be broadened when we add on the bath modes (to anticipate) into a

Lorentzian in energy. The Marcus energy Gaussian form is found when we take account of the *noncommuting* nature of certain (slow) bath electric polarization modes, with the solutes' own instantaneous electrostatic potential.

This remainder can be seen to involve the following terms (ignoring t, because it will soon be integrated out in the F.T. anyway):

$$\exp\left(it'[E_0^N(\mathbf{x}')-E_n^{N+1}(\mathbf{x}')]\right)\exp\left(it'[E_0^N(\mathbf{x}_0)-E_n^{N+1}(\mathbf{x}_0)]\right).$$

So it is clear that the 'poles' of the F.T. will be about $[E_0^N(\mathbf{x}')-E_n^{N+1}(\mathbf{x}')]+[E_0^N(\mathbf{x_0})-E_n^{N+1}(\mathbf{x_0})]$ or $[E_A(\text{product})]-\text{IP}$ (reactant)], where IP(reactant) is the ionization potential of the donor in the presence of the acceptor ('neutral'), and EA (product) is the electron affinity of the acceptor in the presence of the ionized donor. We will write this quantity as $(E_- - E_+)$ (it is here that one correctly interprets the values, in the long time limit, thermodynamically, as the EA of the acceptor and IP of the donor, plus the respective difference in solvation energies – or else the difference in their redox potentials in the given solvent – minus the work required to assemble them together in the solvent, plus the work required to assemble the product D^+ and A^-). These can also be called the 'in' vs. 'out' energy of the complex when referring to their instantaneous energy values.

We average – in the bath modes, and construct a trace over the bath Hamiltonian H_{bath} thus:

$$\begin{aligned}&\text{Tr}\int e^{-\beta\mathsf{H}_{\text{bath}}}G^*(t_1,\,t)\exp(it\mathsf{H}_{\text{bath}}/\hbar)G(t,\,t_1)\exp(-it\mathsf{H}_{\text{bath}}/\hbar)\mathrm{d}E/Z\\&\cong\left\langle e^{-\beta\mathsf{H}_{\text{bath, eff}}}G^*(t_1,\,t)\exp(it\mathsf{H}_{\text{bath, eff}}/\hbar)G(t,t_1)\exp(-it\mathsf{H}_{\text{bath, eff}}/\hbar)\right\rangle_p\end{aligned}\tag{A3}$$

where Z is the partition function $\int e^{-\beta\mathsf{H}_{\text{bath}}}\mathrm{d}E$, and the integral now includes an integration with respect to bath momenta (p). This thermal averaging helps us generate the integral over phase–space paths that we require by moving the origin of paths about in the reactant well. A second kind of averaging, involving a 'centering distribution' is required to select only those paths which approach the barrier region between the two surfaces, as will be seen.

The trace operation then ensures that the same 'effective–Hamiltonian' bath-modes appear together as terms of $\beta\mathsf{H}_{\text{bath,eff}}$ and $\pm i\mathsf{H}_{\text{bath,eff}}t/\hbar$ [42] which can be thought of as further 'dressed' in (A3) with solvent phonons for all the irrelevant modes of the solvent (i.e. those modes which do not participate in reorganization energy, or repolarization energy – *vide infra*).

As mentioned above, the solvent–bath phase–factor and the electron–energy phase factor(s) do not commute, so that – collecting these factors into one exponential – we obtain, via the Campbell–Baker–Hausdorff theorem ($e^{\mathbf{A}}e^{\mathbf{B}}=e^{\mathbf{A}+\mathbf{B}+1/2[\mathbf{A},\mathbf{B}]+\cdots}$), writing $G^*(t,\mathbf{x},0)G(0,t,\mathbf{x}')=P(0)$:

$$\begin{aligned}&\langle e^{-\beta H_{\text{bath,eff}}}P(0)\exp\{i(E_+-E_-)t/\hbar-(1/2[H_{\text{bath}},E_n]\\&\quad+1/2[H_{\text{bath}},E_m])\left(it/\hbar+\beta\right)it/\hbar\}\rangle\end{aligned}\tag{A4}$$

Now, $E_+-E_-/\hbar$ is a frequency, which we will call ω_0, and so if the number integral be multiplied by $e^{-\omega t}$, then we have the Fourier Transform $N(\omega)=Nk(E/\hbar)$ of the expression for $N(t)$.

We make the substitution $t^p=t_1-i\beta\hbar$, and complete the square inside the exponent in (A4). The commutator between solvent energy and electron energy in the region between the reactant and product nuclear potential energy wells where electronic states of either are nearly equal in energy vanishes except for very slow repolarizations, those which cannot equilibrate between the 'in' or 'out' phase of the electron standing wave. The two commutators are then essentially a sum of two-time correlation functions $|U(t^+)U(t_1)|$, and $|U(t^-)U(t_1)|$, which is given by Marcus as the *statistical variance* of the electrostatic energy difference due to linear response in the solvent to the potential obtained from the charge distribution of the solutes.[3] In Marcus' theory [11], this quantity is defined to be $k_BT\lambda$, so that λ is a *linear response* susceptibility [43].

Performing the indicated operations, one finally obtains for '$\langle N(E)\rangle$'[4]:

$$\begin{aligned}\langle N(E)\rangle&=(8\pi\lambda k_BT)^{1/2}/(\hbar(\omega_0-\omega))\langle\exp(\hbar(\omega_0-\omega)/kT)\rangle\\&\quad\langle\exp(-(\hbar(\omega_0-\omega)+\lambda)^2/4k_BT\lambda)\rangle\end{aligned}\tag{A5a}$$

and for the rate $\mathrm{d}\langle N(E)\rangle/\mathrm{d}t$:

$$\begin{aligned}&4\pi\lambda/h\langle\exp(\hbar(\omega_0-\omega)//kT)\rangle\langle\exp(-(\omega_0-\omega\\&\quad+\lambda)^2/4k_BT\lambda)\rangle\end{aligned}\tag{A5b}$$

which is the adiabatic crossing rate ($>>k$ for final separation of the diabatic surfaces), nonetheless the barrier term is correct.

Appendix B

The derivative of the rate with respect to temperature for case A is seen to be:

$$\begin{aligned}\mathrm{d}\ln R/\mathrm{d}T=\{&\mathrm{d}\ln(\rho_0)/\mathrm{d}T+\mathrm{d}\ln(f(T))/\mathrm{d}T+\mathrm{d}\ln\varepsilon_0/\mathrm{d}T\\&+\mathrm{d}\ln(\tau_{\text{diel}}^{-1})/\mathrm{d}T-\mathrm{d}\ln(c)/\mathrm{d}t+w_R^0/k_BT^2\\&+((\Delta F^{0'}+\lambda)^2/4k_B\lambda)1/T^2+\Delta S^*/k_BT\}\end{aligned}\tag{B1a}$$

$$\begin{aligned}\text{or }\mathrm{d}\ln R/\mathrm{d}(1/T)=-T^2\{&\mathrm{d}\ln(\rho_0)/\mathrm{d}T+\mathrm{d}\ln(f(T))/\mathrm{d}T\\&+\mathrm{d}\ln\varepsilon_0/\mathrm{d}T+\mathrm{d}\ln(\tau_{\text{diel}}^{-1})/\mathrm{d}T-\mathrm{d}\ln(c)/\mathrm{d}t\\&+h(T)\mathrm{d}(2K)/\mathrm{d}T+g(T)\mathrm{d}a/\mathrm{d}T\}-w_R^0/k_B\\&-((\Delta F^{0'}+\lambda)^2/4k_B\lambda)-T\Delta S^*/k_B\end{aligned}\tag{B1b}$$

The term $f(T)$, for the record, is equal to $\{1/2+1/2[1+\gamma(T)]^{1/2}\}^{-1}$, with $\gamma(T)=3I\varepsilon_0(\varepsilon_0-1)/(2\pi\tau_{\text{diel}}^2\mu^2\rho_0\varepsilon_\infty^2)$, μ the molecular dipole

[3] In lowest order there are two integrals over charge density distributions for every energy: one that gives the potential as $V(\mathbf{r})=\int\rho/|\mathbf{r}-\mathbf{r}'|\mathrm{d}^3\mathbf{r}'$, with ρ the charge density. The second integral gives the energy$=\int\rho V(\mathbf{r})\mathrm{d}^3\mathbf{r}$ – the variance here is that with one charge density referring to the solvent and the other referring to the donor/acceptor pair.

[4] The Fourier transform allows us to write the full expansion in H_{12} as $N(E)$ $\{1+\zeta^2/(1-\zeta)\}$,[2] where ζ is equal to $\langle H_{12}\rangle/(\sqrt{8\pi\lambda k_BT})$, with $N(E)$ given by Eqs. (A1a) (A1b) (A1c).

moment of the solvent, and I the moment of inertia. The temperature derivatives are given by:

$$\mathrm{d}\ln c/\mathrm{d}T = -\left[|\Delta F^{0\prime}+\lambda|^{-1}+(\Delta F^{0\prime}-\lambda)^{-1}\right]^{-1}\left[|\Delta F^{0\prime}+\lambda|^{-2}+(\Delta F^{0\prime}-\lambda)^{-2}\right]\Delta S^{*}+1/(2T) \quad \text{(B2)}$$

$$\mathrm{d}\ln(f(T))/\mathrm{d}T = -(1+\gamma(T))^{-1/2}/4\, f(T)\mathrm{d}\gamma/\mathrm{d}T;$$
$$\mathrm{d}\gamma/\mathrm{d}T = \gamma(T)[(2+(\varepsilon_0-1)^{-1})\mathrm{d}\ln\varepsilon_0/\mathrm{d}T + 2\mathrm{d}\ln\tau_{\mathrm{diel}}^{-1}/\mathrm{d}T - \mathrm{d}\ln\rho_0/\mathrm{d}T] \quad \text{(B3, B4)}$$

ΔS^{*} is given in the text. In light of our theory that the solvent–electron correlation function does not itself fluctuate, i.e., that the diabatic surfaces are not highly temperature dependent, it seems likely that $\mathrm{d}\ln c/\mathrm{d}T$ should be given instead by $-1/(2T)$ alone for the Calef–Wolynes formula, and $-1/T$ alone for the formula for "c" derived here. The same reasoning leads us to conclude that the polaron density (outside of temperature effects on the solvent cage) may not be highly temperature-dependent.

Note added in Proof

Dougan, Crain, Vass, & Magennis recently (J. Fluorescence, 14, #1, 2004; 91-97) investigated ANS lifetimes in methanol and methanol water mixture to 190K. At the lowest temperatures they found 2 lifetimes, but single lifetimes above 228K.

References

[1] G. Robinson, R. Robbins, G. Fleming, J. Morris, A. Knight, Picosecond studies of the fluorescence probe molecule 8-anilino-1-naphthalenesulfonic acid, JACS 100 (1978) 7145–7150.

[2] E. Kosower, Intramolecular donor–acceptor systems: 9. Photophysics of phenylamino)naphthalenesulfonates: a paradigm for excited-state intramolecular charge transfer, Acc. Chem. Res. 15 (1982) 259–266.

[3] R. Zwanzig, Rate processes with dynamical disorder, Acc. Chem. Res. 23 (1990) 148–152.

[4] H.S. Lin, W. Eyring, A general treatment of relaxation phenomena, PNAS 74 (1977) 3623–3626.

[5] M. Goldberger, K. Watson, Collision Theory, Krieger, Huffington, NY, 1975, pp. 424–440, 1975 reprint from.

[6] P.M. Rodger, M.G. Sceats, Reaction dynamics on a fluctuating potential, J. Chem. Phys. 89 (1988) 5695–5705.

[7] E. Kosower, H. Dodiuk, H. Kanety, Intramolecular donor–acceptor systems: 4. Solvent effects on radiative and nonradiative processes for the charge-transfer states of *N*-arylaminonaphthalenesulfonates, JACS 100 (1978) 4179–4188.

[8] E. Kosower, H. Kanety, Intramolecular donor–acceptor systems: 10. Multiple fluorescences from 8-(phenylamino)-1-naphthalenesulfonates, JACS 105 (1983) 6236–6243.

[9] P. Sadkowski, G. Fleming, The influence of solvent–solute interaction on radiationless processes: excited state dynamics of 1,8-anilinonaphthalene sulphonate and related molecules, Chem. Phys. 54 (1980) 79–89.

[10] G. Robinson, P. Thistlewaite, J. Lee, Molecular aspects of ionic hydration reactions, J. Phys. Chem. 90 (1986) 4224–4233.

[11] R. Marcus, On the theory of electron-transfer reactions: VI. Unified treatment for homogeneous and electrode reactions, J. Chem. Phys. 43 (1965) 679–701.

[12] D. Chandler, Gaussian field model of fluids with application to polymeric fluids, Phys. Rev., E 48 (1993) 2898–2905.

[13] E. Kurian, Solution structure of intestinal fatty acid binding protein complexed with 1-anilinonaphthalene-8-sulfonate: implications for ligand binding, Thesis, Mayo Graduate School of Medicine, Rochester, MN, 1998.

[14] W. Kirk, W. Wessels, F. Prendergast, Lanthanide-dependent perturbation of luminescence in indolylethylenediaminetetraacetic acid–lanthanide chelates, J. Phys. Chem. 97 (1993) 10326–10340.

[15] W. Kirk, E. Kurian, F. Prendergast, Characterization of the sources of protein–ligand affinity: 1-sulfonato-8-anilinonaphthalene binding to intestinal fatty acid binding protein, Biophys. J. 70 (1996) 69–83.

[16] X. Song, A. Stuchebrukov, Outer-sphere electron transfer in polar solvents: quantum scaling of strongly interacting systems, J. Chem. Phys. 99 (1993) 969–978.

[17] D. Calef, P. Wolynes, Classical solvent dynamics and electron transfer: 1, J. Phys. Chem. 87 (1983) 3387–3400.

[18] R. Feynman, A. Hibbs, Quantum Mechanics and Path Integrals, McGraw-Hill, NY, 1965.

[19] D. Chandler, Y. Singh, D. Richardson, Excess electrons in simple fluids: I, J. Chem. Phys. 81 (1984) 1975–1985.

[20] A. Nichols, D. Chandler, Y. Singh, D. Richardson, Excess electrons in simple fluids: II, J. Chem. Phys. 81 (1984) 5109–5116.

[21] A. Nichols, D. Chandler, Excess electrons in simple fluids: III, J. Chem. Phys. 84 (1986) 398–403.

[22] S.H. Glarum, Dielectric relaxation in isoamyl bromide, J. Chem. Phys. 33 (1960) 639–643.

[23] R. Feynman, Slow electrons in a polar crystal, Phys. Rev. 97 (1954) 660–665.

[24] T. Schultz, Slow electrons in polar crystals: self-energy, mass, and mobility, Phys. Rev. 116 (1959) 526–543.

[25] J. Huffaker, P. Dwivedi, Factorization-method treatment of the perturbed Morse oscillator, J. Math. Phys. 16 (1975) 852–867.

[26] P. Morse, Diatomic molecules according to the wave mechanics: II. Vibrational levels, Phys. Rev. 34 (1929) 57–64.

[27] G. Jeffrey, W. Saenger, Study Edition, Hydrogen Bonding in Biological Structures, vol. 28, Springer-Verlag, Berlin, 1994, p. 456.

[28] J. Coe, G. Lee, J. Eaton, S. Arnold, H. Sarkas, K. Bowen, C. Ludewigt, H. Haberland, D. Worsnop, Photoelectron spectroscopy of hydrated electron cluster anions $(H_2O)^-_{n=2-69}$, J. Chem. Phys. 92 (1990) 3980–3982.

[29] T. Ebbeson, C. Ghiron, Role of specific solvation in the fluorescence sensitivity of 1,8 ANS to water, J. Phys. Chem. 93 (1989) 7139–7143.

[30] P. Anderson, Absence of diffusion in certain random lattices, Phys. Rev. 109 (1958) 1492–1499.

[31] A. Antony, C. Smythe, Microwave absorption and molecular structure in liquids: LIII, JACS 86 (1964) 152–156.

[32] R. Kubo, Y. Toyozawa, Application of the method of generating function to radiative and non-radiative transitions of a trapped electron in a crystal, Prog. Theor. Phys. 13 (1955) 160–182.

[33] J. Froehlich, T. Spencer, Absence of diffusion in the Anderson tight binding model for large disorder or low energy, Commun. Math. Phys. 89 (1983) 151–184.

[34] K. Schweizer, D. Chandler, Quantum theory of solvent effects on electronic spectra: predictions of the exact solution of the mean spherical model, J. Chem. Phys. 78 (1983) 4118–4125.

[35] X. Song, D. Chandler, R. Marcus, Gaussian field model of dielectric solvation properties, J. Phys. Chem. 100 (1996) 11954–11959.

[36] R. Marcus, Relation between charge transfer absorption and fluorescence spectra and the inverted region, J. Phys. Chem. 93 (1989) 3078–3086.

[37] N. Nodelman, J. Martin, Solvent cage effect in the photolysis of azomethane in aqueous alcohols and other media: a semiempirical correlation with macroscopic solvent parameters, JACS 98 (1976) 6597–6608.

[38] B. Ladanyi, M. Skaf, Wave vector-dependent dielectric relaxation of methanol–water mixtures, J. Phys. Chem. 100 (1996) 1368–1380.

[39] A. Warshel, W. Parson, Computer Simulations of electron-transfer reactions in solution and in photosynthetic reaction centers, Annu. Rev. Phys. Chem. 42 (1991) 279–309.

[40] W. Greiner, J. Reinhardt, Quantum Electrodynamics, 2nd Ed., Springer Verl, NY, 1996.

[41] P. Jørgenson, J. Simons, Second Quantization-Based Methods in Quantum Chemistry, Acad. Pr., N.Y., 1981.

[42] G. Roepstorff, Path Integral Approach to Quantum Physics, Springer-Verl., 1994, pp. 61–65.
[43] R.Kubo, M. Toda, N. Hashitsume, Statistical Physics II, 2nd ed., Springer Verl., N.Y., 1992, p. 154.
[44] S. Murov, I. Carmichael, G. Hug, Handbook of Photochemistry, 2nd edition, Marcel Dekker, N.Y., 1993.
[45] J. Hasted, Aqueous Dielectrics, Chapman and Hall, London, 1973.
[46] S. Garg, C. Smythe, Microwave absorption and molecular structure in liquids: LXVII, J. Chem. Phys. 46 (1966) 373–377.
[47] M. Sagal, Dielectric relaxation in liquid alcohols and diols, J. Chem. Phys. 36 (1962) 2437–2442.
[48] C. Wohlfarth, "Static Dielectric Constants of Pure Liquids and Binary Liquid Mixtures", in: Landolt–Bernstein: Numerical Data and Functional Relationships in Science and Technology, New Series. ed-in chief G. Madelung, Group IV, Macroscopic and Technical Properties of Matter, vol. 6, Springer-Verl. Berlin 1991.
[49] C. Boettcher, P. Bordewijk, Theory of Electric Polarization: v. II, Elsevier, Amsterdam, 1978.